In vivo magnetic resonance spectroscopy in the brain of Cdkl5 null mice reveals a metabolic profile indicative of mitochondrial dysfunctions

(Article begins on next page)

DR. LINDA CHAABANE (Orcid ID : 0000-0003-2782-9938)

PROF. NICOLETTA LANDSBERGER (Orcid ID : 0000-0003-0820-3155)

Article type   : Original Article

In vivo magnetic resonance spectroscopy in the brain of *Cdkl5* null mice reveals a metabolic profile indicative of mitochondrial dysfunctions

Sara Carli[1§], Linda Chaabane[2§], Clarissa Butti[1,3], Clara De Palma[4], Patrizia Aimar[5], Chiara Salio[5], Aglaia Vignoli[6], Maurizio Giustetto[7,8], Nicoletta Landsberger[1,4*], Angelisa Frasca[4*]

[1]Neuroscience Division, IRCCS San Raffaele Scientific Institute, Milan, I-20132, Italy; carli.sara@hsr.it (S.C.); landsberger.nicoletta@hsr.it (N.L.)

[2]Institute of Experimental Neurology (INSPE) and Experimental Imaging Center (CIS), IRCCS San Raffaele Scientific Institute, Milan, I-20132, Italy; chaabane.linda@hsr.it (L.C.)

[3]Molecular Nociception Group, Wolfson Institute for Biomedical Research (WIBR), University College London, London, WC1E6BT, United Kingdom; c.butti@ucl.ac.uk (C.B.)

[4]Department of Medical Biotechnology and Translational Medicine, University of Milan, Segrate (Milan), I-20090, Italy; clara.depalma@unimi.it (C.D.P.); angelisa.frasca@unimi.it (A.F.); nicoletta.landsberger@unimi.it (N.L.)

[5]Department of Veterinary Sciences, University of Turin, Grugliasco, I-10095, Italy; patrizia.aimar@unito.it (P.A.); chiara.salio@unito.it (C.S.)

[6]Epilepsy Center-Child Neuropsychiatric Unit, ASST Santi Paolo e Carlo, Department of Health Sciences, University of Milan, Milan, Italy; aglaia.vignoli@unimi.it (A.V.)

[7]Department of Neuroscience, University of Turin, Turin, I-10126, Italy; maurizio.giustetto@unito.it (M.G.)

[8]National Institute of Neuroscience-Italy, Turin, I-10126, Italy

§ Co-first authors

* Corresponding authors: Nicoletta Landsberger (ORCID 0000-0003-0820-3155) and Angelisa Frasca (ORCID 0000-0002-0963-9789)

Running title: MRS uncovers mitochondrial deficits in the CDD brain

Keywords: *CDKL5* deficiency disorder (CDD), *Cdkl5* mouse model, MRI/MRS studies, biomarkers, mitochondria, 5'-AMP-activated protein kinase

Abbreviations:

AMPK: 5'-AMP-activated protein kinase

ASD: Autism Spectrum Disorders

CDD: CDKL5 deficiency disorder

CDKL5: cyclin-dependent kinase-like 5

EP: entorhinal-perirhinal cortex

ETC: electron transport chain

HET: heterozygous

KO: knock-out

MEMRI: Manganese Enhanced Magnetic Resonance Imaging

MRI: Magnetic Resonance Imaging

MRS: Magnetic Resonance Spectroscopy

MT: mitochondria

PF: parafascicular nucleus

VC: visual cortex

VEP: Visual Evoked Potential

VP: ventral posterior nucleus

WT: Wild type

Abstract

Mutations in the X-linked *CDKL5* gene cause CDKL5 deficiency disorder (CDD), a severe neurodevelopmental condition mainly characterized by infantile epileptic encephalopathy, intellectual disability and autistic features. The molecular mechanisms underlying the clinical symptoms remain largely unknown and the identification of reliable biomarkers in animal models will certainly contribute to increase our comprehension of CDD as well as to assess the efficacy of therapeutic strategies. Here, we used different Magnetic Resonance (MR) methods to disclose structural, functional or metabolic signatures of *Cdkl5* deficiency in the brain of adult mice. We found that loss of *Cdkl5* does not cause cerebral atrophy but affects distinct brain areas, particularly the hippocampus. By *in vivo* proton-MR spectroscopy (MRS), we revealed in the *Cdkl5* null brain a metabolic dysregulation indicative of mitochondrial dysfunctions. Accordingly, we unveiled a significant reduction in ATP levels and a decrease in the expression of complex IV of mitochondrial electron transport chain. Conversely, the number of mitochondria appeared preserved. Importantly, we reported a significant defect in the activation of one of the major regulators of cellular energy balance, the adenosine monophosphate-activated protein kinase (AMPK), that might contribute to the observed metabolic impairment and become an interesting therapeutic target for future preclinical trials.

In conclusion, MRS revealed in the *Cdkl5* null brain the presence of a metabolic dysregulation suggestive of a mitochondrial dysfunction that permitted to foster our comprehension of *Cdkl5* deficiency and brought our interest towards targeting mitochondria as therapeutic strategy for CDD.

Introduction

Mutations in the X-linked cyclin-dependent kinase like 5 gene (*CDKL5*) cause a rare neurologic condition designated CDD (CDKL5 deficiency disorder; OMIM 300203, 300672) that affects children of both genders and is generally characterized by onset of seizures in the first weeks to months of life and severe intellectual disability (Fehr et al., 2013; Demarest et al., 2019). With an estimated incidence of 1 in 40-60,000 live births, CDD represents one of the most common genetic cause of epilepsy in infants (Kothur et al., 2018; Lindy et al., 2018). CDD patients manifest additional symptoms including severe hypotonia, autistic features and stereotyped hand movements, disrupted sleep, gastrointestinal problems, dysautonomia and cortical visual impairment (CVI) (Bahi-Buisson et al. 2008; Hagebeuk et al., 2012; Mangatt et al. 2016).

The recent generation of mouse models of *Cdkl5* deficiency is revealing instrumental to determine the main role(s) of *Cdkl5* in brain development and the effects of its mutations on neuronal and synaptic functions (Wang et al., 2012; Amendola et al., 2014; Jhang et al., 2017; Okuda et al., 2017; Tang et al., 2017; Schroeder et al., 2019). Although CDD affects mainly females, studies are often performed on hemizygous mutant male mice that present more robust and consistent phenotypes with respect to heterozygous animals. Generally, *Cdkl5* deficient mice exhibit several behavioural phenotypes mimicking primary features of autism, such as impaired learning and memory, social interaction, communication and motor coordination together with increased stereotypy. Interestingly, these mouse models share with CDD patients also cortical visual defects (Pizzo et al., 2016; Mazziotti et al., 2017). Concerning spontaneous seizures, it has recently been proved that aged heterozygous $Cdkl5^{+/-}$ females recapitulate multiple features of epilepsy manifested by CDD patients (Mulcaheya et al., 2020), while *Cdkl5* null male mice exhibit enhanced seizure susceptibility in response to NMDA treatment (Okuda et al., 2017).

Investigations on *Cdkl5* mouse models have been and still are pivotal to understand the association of the observed phenotypes with Cdkl5 localization and the neurobiological alterations caused by its deficiency. Indeed, both in humans and mice, the protein is abundantly expressed in brain,

predominantly in forebrain, hippocampus and striatum, three cerebral regions critically important for cognition, social behaviours, motor planning and decision making. In contrast, in thalamus, a key area for motor and sensory functions, CDKL5 levels are less abundant (Rusconi et al., 2008; Wang et al., 2012). In addition, it has been demonstrated that the lack of *Cdkl5* in neurons affects dendritic morphology, axon outgrowth, spine density, excitatory synaptic transmission and plasticity (Zhu and Xiong, 2018), therefore leading to numerous functional changes at the synaptic and circuit levels (Della Sala et al., 2016; Okuda et al., 2017; Tang et al., 2017). Besides being useful to reveal the cellular and molecular origins of CDD-related phenotypes, CDD mouse models have also permitted to initiate preclinical studies investigating pharmacological and molecular therapies (Della Sala et al., 2016; Fuchs et al., 2018; Vigli et al., 2019). However, assessment of treatment efficacy strongly depends on the availability of biomarkers able to quantitatively measure structural, functional, metabolic or molecular impairments and their disease-modifying potential. So far, it has been demonstrated that visual cortical responses mainly assessed by visual evoked potential (VEP) recordings can be used as a non-invasive biomarker of disease progression in *Cdkl5* null mice (Mazziotti et al., 2017), an objective outcome that can also be applied for CDD patients' follow up (Demarest et al., 2019).

Magnetic Resonance Imaging (MRI) is a key imaging technique for localizing and quantifying anatomical, functional and metabolic alterations in different neurological diseases that could reveal pathophysiologic features of CDD both in human and mouse brains.

Although brain MRI is routinely performed in infants at seizure onset, MRI data are available on few CDD patients, with contrasting results. Indeed, while the absence of structural anomalies in the CDD brain is generally reported at early phase of the disorder, a progressive cerebral atrophy, including thinning of the white matter and abnormal myelination, has been seldom described (Bahi-Buisson et al., 2008; Artuso et al., 2010; White et al., 2010; Mirzaa et al., 2013; Liang et al., 2019). Whether these phenotypes predominate in CDD male patients is still debated (Liang et al., 2019). To the best of our knowledge, no comprehensive study using MR approaches has been done on cerebral metabolism in CDD patients; further, no MRI investigation on *Cdkl5* defective mice has ever been reported.

In the present work, we have used different MR methods to assess in adult *Cdkl5* mutant mice whether brains suffer from structural, functional or metabolic impairments. In particular, we have performed *ex vivo* and *in vivo* MRI to analyse brain morphology while we have investigated the neurochemical signature produced by *Cdkl5* loss by proton-MR Spectroscopy (^{1}H-MRS). Because mapping metabolites *in vivo* in the entire brain is challenging, regions of interest have to be defined before the acquisition of MR spectra. To select the cerebral areas showing major dysfunctions, we have exploited the manganese-enhanced MRI (MEMRI), a method used in pre-clinical studies to highlight neuronal activity (Duong et al., 2000; Silva and Bock, 2008).

Our findings suggest that both *Cdkl5* null and heterozygous adult mouse brain structure is not primarily affected by the lack of *Cdkl5*, thus confirming previous data suggesting the absence of cerebral atrophy in CDD mice (Amendola et al., 2014). Intriguingly, we have revealed that *Cdkl5* deficiency affects neuronal activity in several brain areas, particularly in the hippocampus and part of the visual system. MRS studies have disclosed various metabolic dysregulations in the *Cdkl5* null hippocampus supporting previous indications of defective energy metabolism and mitochondrial functions (Jagtap et al., 2019; Vigli et al., 2019). We have improved these data proving that the *Cdkl5* KO hippocampus suffers from reduced ATP levels, together with significant defects in AMPK activation and in the expression of complex IV of mitochondrial electron transport chain (ETC).

Materials and Methods

Animals

All procedures were performed in accordance with the European Community Council Directive 2010/63/UE for care and use of experimental animals with protocols approved by the Italian Government (decrees No. 210/2017-PR and 175/2015-PR), the San Raffaele Scientific Institutional Animal Care and Use Committee and the Bioethics Committee of the University of Torino. Institutional ethical approval was not required for this study. The study was not pre-registered.

Mice used in all experiments of this work (Figure 1) derive from the *Cdkl5* null mouse strain described in Amendola et al., 2014, a conventional knock-out lacking exon 4. The strain was generated on a C57BL/6J background and was kindly donated by Dr Elisabetta Ciani (University of Bologna) to NL.

In two recent papers (Cobolli Gigli et al., 2016; Gandaglia et al., 2018), we have proved the advantages of maintaining mouse models of *Mecp2* on an outbred CD1 background that is characterized by a significant robustness and the production of large litters. We considered these features an advantage to foster research on CDD. Therefore, we crossed C57BL/6J *Cdkl5* heterozygous females with CD1 WT male mice (Crl:CD1 (ICR); Charles River) and kept backcrossing each generation of heterozygous females with new CD1 WT males. This backcrossing strategy occurred for more than 10 generations. The generated knock out line generally recapitulates the behavioural phenotypes exhibited by the same line maintained on an inbred background. These animals have already been cited in few recent publications (Balestra et al., 2019; Barbiero et al., 2020; Trovò et al., 2020).

CD1 *Cdkl5* mice were used for most of the experiments (MRI analysis, CellTiter Glo, qPCR and Western Blot), while C57Bl/6J line was used for the electron microscopy (EM) analyses shown in Supplementary Figure 2. C57BL/6J mice were obtained by mating $Cdkl5^{-/x}$ heterozygous females with $Cdkl5^{-/y}$ male mice. The genetic background of all results is clearly indicated in the text. Mouse genotype was determined by PCR protocol on genomic DNA purified from ears using the following primers: forward primer for the null allele 5'-ACGATAGAAATAGACGATCAACCC-3'; forward primer for the WT allele 5'-CCCAAGTATACCCCTTTCCA-3'; common reverse primer 5'-

CTGTGACTAGGGGCTAGAGA-3'. Mice were housed in groups of four in Tecniplast cages (cat.no. 1144b-001), on a 12 h light/dark cycle in a temperature-controlled environment (21 $\pm$ 2 °C) with food and water provided *ad libitum*. Animals were weighed before starting the study. The general health of mice was evaluated twice a week and no sign of stress or suffering (i.e. signs of irregular respiration or tremor; evaluation of grooming, hair coat and eyes; checking of motor postures, gait or clasping; changes in body weight) was observed. Mouse handling was performed only by professional and trained experimenters, in order to reduce stress manipulation. A total of 86 adult animals were included in the study (Figure 1; males n = 30 KO and 38 WT at P70 days, females n=10 HET and 8 WT at P160-195 days). At these ages CD1 adult male and heterozygous female mice show similar behavioral features (Fuchs et al., 2018; Okuda et al., 2018). Heterozygous female mice between 5.3 to 6.5 months of age were included in the study. Importantly, all animals belonging to the same experimental group always showed similar conditions. Littermate controls were used for all the experiments.

Magnetic Resonance Imaging, Magnetic-Enhanced MRI and Spectroscopy (MRI, MEMRI and MRS)
All MRI experiments were conducted on a 7-Tesla scanner for rodents, fully equipped for brain MRI/MRS (Biospec, Paravision 6.0 Software Bruker-Biospin). A dedicated mouse head coil (4-channels) was used as receiver together with a volume coil as transmitter.

For *ex vivo* MEMRI, animals were treated with manganese chloride (MnCl$_2$ pH=7.4, 60 mg/kg, intraperitoneal administration) 24 hours before sacrifice. Manganese ion (Mn^{2+}) enters into excitable cells via calcium channels, therefore accumulating in active cerebral regions, which are revealed by MRI through the reduction of the T1 relaxation time (Duong et al., 2000; Itoh et al., 2008; Silva and Bock, 2008). For both female and male groups, a control mouse of the corresponding gender (blank) was treated with an equal dose of sodium chloride (0.9% NaCl) and used as reference for manganese uptake quantification. The day after manganese treatment, animals were deeply anesthetized by a single intraperitoneal injection of Avertin (250 mg/Kg, Sigma-Aldrich, cat.no. T48402), already used to induce deep anaesthesia before the sacrifice in *Cdkl5* KO mice (Amendola et al., 2014; Lupori et al., 2019; Pizzo et al., 2016). The use of Avertin followed approval of the experimental protocols by the Italian Government (decrees No. 210/2017-PR and 175/2015-PR) and the drug has been stored

and applied according to the manufacturer's instruction to avoid irritations that may be caused by incorrect storage. Following a deep anaesthesia, the experimenter verified that every reflex of the animal was absent by pinching the tail. Then, mice were transcardially perfused with 100 mM PBS pH=7.4, followed by 4% paraformaldehyde (PFA). The brains were carefully removed from the skull, kept in 4% PFA for 24 h and then conserved in 100 mM PBS supplemented with 0.02% sodium azide for one week before MRI acquisition. All animals of the study were sacrificed in the morning.

For *ex vivo* MRI, fixed brains were placed over a support of agar gel (2%) and positioned under the mouse brain coil. T2 weighted MR images were acquired with coronal sections of 0.7 mm and an in plane resolution of 83 μm (matrix = 192, FOV = 16 mm) using a fast-spin-echo sequence (TR/TE = 3500/45 ms, rare factor = 8, average = 8, 11 minutes of acquisition) ($MnCl_2$ or NaCl treated mice; males: n = 5 KO and 6 WT littermates; females: n = 10 HET and 8 WT littermates; CD1 background). To quantify manganese uptake (MEMRI), a map of the longitudinal relaxation time T1 was acquired using a spin-echo sequence with different recovery times (n = 6, 290 to 4000 ms, TE= 6.65 ms, 49 minutes of acquisition) and a resolution of 103 μm with sections similar to T2 weighted images (0.7 mm of thickness). The complete MRI exam lasted 80 minutes for each sample. Maps of T1 were calculated using the mono exponential fitting tool of Paravision. The contrast enhancement of manganese was calculated as the percentage of relaxivity (R1 = 1/T1) differences versus blank mice (0.9% NaCl treated; same gender of the experimental group). Manganese uptake was measured in several brain areas identified through the reference atlas from Allen Institute for Brain Science (http://atlas.brain-map.org/).

For *in vivo* MRI, a mixture of IsoVet (isoflurane 1-2%; Zootecnica, cat.no. 104331020) with oxygen was used to anaesthetize animals (n = 8 KO and 7 WT male littermates; CD1 background) and breath rate was continuously monitored to adjust the level of anaesthesia. IsoVet is an inhalation anaesthetic commonly used for general anaesthesia in animals. Induction and recovery from anaesthesia with isoflurane are rapid. Body temperature of mice was maintained through warm water circulating inside the bed. T2-weighted images of the entire brain were acquired with a fast-spin-echo sequence (TR/TE= 3350/44 ms, resolution of 73 μm, thickness of 0.65 mm, 9 averages, 8 minutes of acquisition). For proton MR spectroscopy (^{1}H-MRS), a PRESS sequence (TR/TE = 2000/16.1 ms) was used to allow the selection of a voxel either in the hippocampus (size = $1.15 \times 1.3 \times 2.65$ mm³) or in

the thalamus (size = $1.5 \times 1.8 \times 1.9$ mm^3) with water-suppression (VAPOR) and the signal was accumulated for 400 and 300 times for each area (10-13 minutes of acquisition), respectively. For each area, magnetic field homogeneity was optimized through the use of automatic map-shim calculation from a B0 map initially acquired. A spectrum with no water suppression was also acquired and used for metabolites concentration calculation using the LCModel program (http://s-provencher.com/lcmodel.shtml). All acquired spectra were obtained with a suitable signal to noise ratio (mean ± st.dev = 8 ± 3) allowing the quantification of more than 12 metabolites (Supplementary Table S1). Metabolites with an estimated standard deviation (Cramer-Rao lower bounds, %SD) higher than 27% were excluded. Indeed, the considered metabolites were estimated with a %SD = 10 ± 6 (mean ± st.dev over all metabolites).

From each T2-weighted MRI data, the total brain volume was calculated from brain area segmentation using the image analysis tools from Paravision. A total of 10 (*ex vivo*) and 23 (*in vivo*) MR sections acquired along the brain were used. For the *ex vivo* studies, olfactory bulbs and cerebellum were excluded from the analyses as they were partially damaged during brain extraction procedures. For *in vivo* MRI, ventricles areas were also quantified and subtracted from the total brain volume. Such exclusion was not possible for *ex vivo* analysis since ventricles were collapsed post-fixation.

RNA Purification, cDNA Synthesis and quantitative RT-PCR

CD1 *Cdkl5* deficient mice and WT littermates were sacrificed by dislocation and brains were rapidly removed (P70 males: n = 15 WT and 8 KO, including those that underwent MRS). Hippocampus was dissected out and immediately frozen on dry-ice and conserved at -80°C until analysis. Total RNA was extracted using Purezol (Bio-Rad, cat.no. 7326890) and mechanical trituration of the tissue was performed using a glass-glass potter. RNA was quantified using a NanoDrop 1000 spectrophotometer and integrity verified by agarose electrophoresis. First strand cDNA was synthesized using the RT2 First Strand Kit (Qiagen, cat.no. 330404) as instructed by the manufacturer and used as a template for quantitative RT-PCR with SYBR Green Master Mix (Applied Biosystems, cat.no. 4472908).

The following primers were used:

Atp5a1	5'- GCCATCGTGGATGTCCCCGTTG-3'; 5'- CTTTCAGGCCCACTCGTCTGCG-3'	Nuclear encoded gene	ETC nuclear subunit (Complex V)
Cox-7b	5'-TTGCCCTTAGCCAAAAACGC-3'; 5'- TCATGGAAACTAGGTGCCCTC-3';	Nuclear encoded gene	ETC nuclear subunit (Complex IV)
Ndufv2	5'-GCAAGGAATTTGCATAAGACAGC-3'; 5'-TAGCCATCCATTCTGCCTTTG-3';	Nuclear encoded gene	ETC nuclear subunit (Complex I)
Sdha	5'- AGCAAGCTCCTGCCTCTGTGGT -3'; 5'- GCTCTGTCCACCAAATGCACGCT-3'	Nuclear encoded gene	ETC nuclear subunit (Complex II)
Slc25a12	5'-ATGGCGGTCAAGGTGCATAC-3'; 5'-AGTCATGTAATGCTCCCCGTC-3';	Nuclear encoded gene	Solute Carrier Family 25 Member 12
Slc25a27	5'-CCACCCACGGCTTATCCAG-3'; 5'-ACAAAAGTCCCCTTCCTTGTTT-3';	Nuclear encoded gene	Solute Carrier Family 25 Member 27
Uqrc1	5'-AGACCCAGGTCAGCATCTTG-3'; 5'-GCCGATTCTTTGTTCCCTTGA-3'	Nuclear encoded gene	ETC nuclear subunit (Complex III)

Melting curve showed a single product peak, indicating good product specificity. All samples were analysed in triplicate and mRNA levels were normalized to *Hprt* (forward primer 5'-ACAGGCCAGACTTTGTTGGAT-3'; reverse primer 5'-TGCAGATTCAACTTGCGCTC-3') as internal standard. Fold change in gene expression was calculated using the 2(-ΔCt) method (Livak & Schmittgen, 2001).

For mitochondrial DNA (mtDNA) analysis, total genomic DNA was isolated from hippocampus of CD1 *Cdkl5* KO (n = 5) and WT littermates (n = 6). The tissues were digested in 200 µl of Digestion Buffer (50 mM Tris-HCl pH 8, 100 mM EDTA pH 8, 100 mM NaCl, 1% SDS) and Proteinase K (Genespin, cat.no. STS-OK500, 0.1 µg/µl) overnight at 55°C. Then, 200 µl of Phenol/Chloroform/Isoamyl alcohol (25:24:1, Sigma-Merck, cat.no. P3803) was added and samples were centrifuged at 13000 x g at room temperature for 10 minutes. The aqueous phase was drawn and 2.5 Vol µl of EtOH absolute + 1:10 Vol of 3M Sodium Acetate was added. After centrifugation at 13000 x g at room temperature for 10 minutes, the supernatant was removed. The pellet was resuspended in 100 µl of milliQ H_2O and let overnight at 55°C. Subsequently, mtDNA and nuclear

DNA were measured by qPCR using primers for *CytB* (forward primer 5'-ACGCCATTCTACGCTCTATC-3'; reverse primer 5'-GCTTCGTTGCTTTGAGGTGT-3') and *Rnase P* (forward primer 5'-GAAGGCTCTGCGCGGACTCG-3'; reverse primer 5'-CGAGAGACCGGAATGGGGCCT-3') content, respectively. DNA (20 ng/well) was mixed with SYBR Green Master Mix (Applied Biosystems, cat.no. 4472908) and primers. The following formula: ΔCt = mean value of Ct(mDNA)/mean value of Ct(nDNA) was used in each sample and results are presented as percentage of WT.

Western Blot

Western blots were performed on hippocampi derived from CD1 mice (n = 10 WT and 9 KO, including contralateral tissues of some animals used for qPCR; Figure 1). Hippocampal tissues were dissected and homogenized in 400 μl of RIPA buffer (100 mM Tris HCl pH 7.5, 300 mM NaCl, 10 mM EDTA, 2% NP-40, 0.2% SDS, 1% sodium deoxycholate) containing Protein Inhibitor Complex 1X (Sigma Merck, cat.no. P8340) and PhosSTOP (Sigma Merck, cat.no. 4906845001). Samples were centrifuged at 12000 x g for 30 min at 4°C and supernatants were collected and stored at -80°. Protein concentrations were calculated using bicinchoninic acid (BCA) assay kit (Thermo Scientific, cat.no. 23228); 10 or 30 μg of protein extract were loaded onto TGX Stain-Free gel prepared by FastCast Acrylamide Kit (Bio-Rad, 10%: cat.no. 1610183; 12%: cat.no. 1610185; 4-15%, cat.no. 5678084). Before transfer, a Stain-Free gel image was acquired by ChemiDoc Touch Imaging System (Bio-Rad) and used to quantify results. Proteins were blotted on a nitrocellulose membrane (Trans-blot Turbo Nitrocellulose Transfer Packs, Bio-Rad Mini cat.no. 1704159 and Bio-Rad Midi cat.no. 1704158) using the Trans-blot SD (Bio-Rad) semidry apparatus. Membranes were incubated at room temperature for 1 hour in blocking solution (Tris-buffered saline containing 0.1% Tween-20 (TBS-T) and 5% nonfat milk or 3% BSA [Sigma Merck, cat.no. A30659]) before adding primary antibodies at the proper dilution: anti-total OXPHOS (Abcam, cat.no. ab110413; 1:1000 in 3% BSA in TBS-T); anti-AMPK-alpha2 (Cell Signaling, cat.no. 2532; 1:1000 in 5% milk in TBS-T); anti-phospho-AMPK-alpha2 (Thr172) (Cell Signaling, cat.no. 2535; 1:1000 in 5% milk in TBS-T); anti-Aralar B-2 (Santa Cruz, cat.no. sc-271056; 1:1000 in 5% milk in TBST); anti-UCP4 (Invitrogen, cat.no. PA5-110384, 1:1000 in 5% milk in TBS-T). After 3 washes in TBS-T, blots were incubated with the

appropriate HRP-conjugated secondary antibody (Peroxidase-conjugated AffiniPure Goat anti-mouse or rabbit IgG (H+L), mouse cat.no. 115-035-003, rabbit cat.no. 111-035-144, Jackson ImmunoResearch) appropriately diluted in 5% milk or 3 % BSA in TBS-T. Immunocomplexes were visualized using the ECL substrates kits from Cyanagen and the Bio-Rad ChemiDoc™ System. Quantification of bands was performed using the Image Lab 5.2.1 Software.

ATP measurement

A luminescence assay (CellTiter-Glo Luminescent Cell Viability Assay, Promega, cat.no. G7570) was used to determine ATP content (Chida et al., 2012) in *Cdkl5* KO mouse (n = 5) and WT littermates (n = 5). Some of these tissues correspond to the contralateral hippocampus of animals used for MRS (Figure 1). Specifically, frozen tissues were homogenized in 0.3 ml of cold lysis buffer (0.25 M sucrose, 10mM HEPES-NaOH pH 7.4), with ultra-turrax (10 sec at max speed) and the homogenates were cleared by centrifugation at 1000 x g, 4°C, 10 min. 250 µl of supernatant was quickly added to an equal volume of ice-cold 10% trichloroacetic acid (TCA), shaken for 20 sec and then centrifuged 10 min at 10.000 x g at 4°C. After TCA extraction, TCA was neutralized adding 200 µl of Tris-acetate buffer (1M pH 8) to 400 µl of supernatant. Following a 10-fold dilution with deionized water, the extract was used for luciferase-luciferin assay. The reaction mix, containing luciferase and substrate, was added and the light emission was measured using a GloMax luminometer (Promega) and quantified according to an ATP standard curve.

Statistical analysis

Structural analysis of mitochondria was performed by an experimenter blinded to the genotype, while for MRI and molecular experiments no blinding was performed. No statistical method was used to calculate sample size, which was determined based on the previous experience of the group with the goal to minimize the number of animals required. Also, no randomization was performed to allocate animals. In MRS, metabolites with an estimated standard deviation (Cramer-Rao lower bounds, %SD) higher than 27% were considered as outliers. Grubb's test was used to determine the presence of significant outliers in Western blot experiments, while, in qPCR experiments, samples in which *Hprt* triplicates average was 0.3 Ct apart from the others were excluded from the analysis. By using these

criteria, n = 1 KO animal was excluded from Western blot experiments and n = 1 KO from qPCR experiments. Some animals were excluded from the MEMRI analysis either due to perfusion fixation artefacts or manganese contrast administration (n = 1 KO and 1 WT males; n = 2 HET and 2 WT females). In order to use the correct statistical test, we first evaluated the normal distribution of data by applying the D'Agostino-Pearson normality test. In accordance with data distribution, Student's t test or Mann-Whitney test were used for the statistical analysis with GraphPad Prism 8 software (LaJolla, CA, USA). For *ex vivo* MEMRI, data collected from left and right hemispheres were averaged. Statistically significance was expressed as: * $p < 0.05$, ** $p < 0.01$, *** $p < 0.001$ and **** $p < 0.0001$ and reported data are mean ± SEM. Multivariate statistical analyses on metabolite data set were performed using the web-based platform MetaboAnalyst (www.metaboanalyst.ca). Autoscaling was applied to the data set prior to perform Partial Least Squares Discriminant analysis (PLS-DA). Successively, metabolites contributing most to group separation were defined from the VIP (variable importance for the projection) scores > 1.2 (Xia & Wishart, 2011).

Results

Cdkl5 KO and HET adult mice do not exhibit brain atrophy
MRI represents a promising non-invasive approach to investigate neurological diseases in animal models, however to date no *in vivo* imaging study has been reported in the *Cdkl5* mouse model. We used MRI in *Cdkl5* mutant mice (Amendola et al., 2014) to identify morphological defects and to unveil the most affected brain regions. This analysis was performed on CD1 adult hemizygous male (P70) and heterozygous female (P160-195) mice, i.e. at an age with similar behavioral features between genders (Fuchs et al., 2018; Okuda et al., 2018). Of note, for all the animals included in the study, no difference in body weight was found between groups (mean grams ± SEM: 40.6 ± 0.4 vs 40.5 ± 0.7 in *Cdkl5* KO vs WT males and 43.6 ± 1.9 vs 45.3 ± 1.4 in *Cdkl5* HET vs WT females).

Brain size of *Cdkl5* KO and HET mice was measured by MRI, in both *ex vivo* and *in vivo* analyses, and compared to the corresponding controls. Cerebral volume was assessed by measuring the total brain area from MR sections acquired along the brain (10 sections for *ex vivo* and 23 sections for *in vivo*). In good accordance with previous studies performed on the same mouse line but in a C57Bl/6J background (Amendola et al., 2014), we did not found morphological alteration in mutant mouse

brains. Indeed, in both mutant male and female animals, the total cerebral area, measured *ex vivo*, was perfectly analogous to their corresponding WT controls (Figure 2A) and no statistical difference was found in total brain volume and brain weight (Figure 2B, C). Accordingly, *in vivo* studies on P70 male mice confirmed the lack of alteration in cerebral size of *Cdkl5* KO mice (Figure 2D, E).

Manganese-Enhanced Magnetic Resonance Imaging (MEMRI*) indicates cellular dysfunction in Cdkl5 deficient brains*

In order to assess how and where *Cdkl5* deficiency affects cerebral function, brains from KO (P70) and HET (P160-195) CD1 mice were analyzed by MEMRI, that could provide a map of neuronal activity (Duong et al., 2000; Silva and Bock, 2008). After the systemic administration of $MnCl_2$, a pronounced contrast enhancement all over the brain due to Mn^{2+} accumulation was observed in treated mice compared to the blank (saline-treated animals) (Figure 3A). Since Mn^{2+} can enter excitable cells through the voltage-gated calcium channel $Ca_v1.2$ and NMDA receptor, an increase in Mn^{2+} intracellular concentration should be indicative of cerebral dysfunctions (Duong et al., 2000; Silva and Bock, 200; Itoh et al., 2008).

Interestingly, the manganese contrast was considerably increased in KO and HET brains compared to the corresponding WT (Figure 3B). Of note, the increase in Mn^{2+} uptake through cerebral regions was not uniformly distributed, highlighting the relevance of MEMRI to identify differences among regions and to unveil the most affected ones (Table 1). Importantly, in KO mice, a significant Mn^{2+} uptake was measured overall the hippocampus (p = 0.0286), an area commonly affected in CDD (Fuchs et al., 2014; Okuda et al., 2017; Tang et al., 2017). This contrast enhancement was uniformly distributed in the different hippocampal areas, including the dentate gyrus (41.5% ± 6.7 with respect to WT), and both stratum lacunosum-moleculare (38.5% ± 6.6) and stratum radiatum (41.0% ± 3.7%) of CA1. Conversely, only a trend toward higher Mn^{2+} enhancement was observed in the hippocampus of HET mice.

However, by analyzing different portions of the cerebral cortex, we reported differences in manganese contrast in both genders. In fact, an increasing trend toward enhancement was observed in auditory cortex (KO: p = 0.0286 and HET: p = 0.0177), which is related to the sensory-motor processing cycle (King et al., 2018), in the posterior parietal association cortex (KO: p = 0.057 and HET: p = 0.202),

involved in decision-making following a visual stimuli (Pho et al., 2019) and in the entorhinal-perirhinal cortex (EP) (KO: p = 0.114 and HET: p = 0.0025), important in the visual recognition memory and whose association with *Cdkl5* loss was already investigated (Ren et al., 2019).

In contrast, only a minor Mn^{2+} enhancement was observed in the thalamus. Indeed, in the parafascicular nucleus (PF) and in the ventral posterior nucleus (VP), Mn^{2+} contrast showed a tendency toward an increase both in KO and HET mice, without being statistically significant (VP, KO: p = 0.114 and HET: p = 0.106; PF, KO: p = 0.114 and HET: p = 0.149).

Moreover, since previous studies reported an impairment in the visual system of CDD patients and animal models (Moseley et al., 2012; Pizzo et al., 2016; Ren et al., 2019; Lupori et al., 2019), we also analyzed the principal nodes related to the visual circuit: optic tract, superior colliculus, visual cortex and the EP. Interestingly, a significant contrast enhancement was measured in the superior colliculus of both mutant groups (KO: p = 0.0286 and HET: p = 0.0303) and selectively in the visual cortex of the HET group (KO: p = 0.114 and HET: p = 0.0025), with no difference in the optic tract.

Interestingly, in the hypothalamus, the increase in Mn^{2+} uptake showed a near-significant trend in KO (p = 0.057), but not in HET mice (p = 0.432).

To summarize, MEMRI suggests that *Cdkl5* deficiency particularly affects cerebral areas associated with memory, cognitive, sensory and motor processes, with differences between genders and brain regions; further it highlights the hippocampus as the most affected area.

In vivo MRS reveals metabolic dysregulation in Cdkl5 KO mice

Considering the higher variability of the phenotype in heterozygous females due to X chromosome inactivation, we decided to explore the cerebral metabolism through *in vivo* MR spectroscopy (MRS) only in KO animals, thus avoiding confounding results due to the mosaic expression of the mutant *Cdkl*5 allele in females.

Based on MEMRI results and literature evidence that associate most of *Cdkl*5 dysfunctions to the hippocampus, MRS was initially performed in this area (Figure 4A-E). Furthermore, to confirm the potential of MEMRI to identify the most involved brain areas in CDD, we selected a cerebral region in which manganese accumulation was less prominent. We thus analyzed the neurochemical profile also in thalamus, an important center of sensory inputs (Figure 4F-J). Although potentially relevant,

the visual system was not included in the study since the MR signal was too low for metabolite quantification.

MRS was acquired in a single hemisphere (left hippocampus, Figure 4A, and right thalamus, Figure 4F) since no difference of manganese uptake was found between left and right of each selected cerebral area.

The following cerebral metabolites were quantified: creatine with phosphocreatine (Cr+PCr), gamma-aminobutyric acid (GABA), glutamine (Gln), glutamate (Glu), glutathione (GSH), glycerophosphocholine with phosphocholine (GPC+PCh), lactate (Lac), myo-Inositol (Ins), N-acetyl aspartate (NAA), N-acetyl-aspartate with N-acetyl-aspartyl-glutamate (NAA+NAAG), phosphocholine (PCh), phosphocreatine (PCr) and taurine (Tau) (Supplementary Table S1).

Score plots derived from Partial Least Squares Discriminant Analysis (PLS-DA) permitted to appreciate a separation of metabolic profiles derived from *Cdkl*5 KO animals and WT littermates both in hippocampus and thalamus (Figure 4B, G). Metabolites that mainly contributed to the cluster discrimination were identified by a high variable importance for the projection (VIP score >1.2) (Figure 4C, H). Interestingly, most of these metabolites were downregulated in *Cdkl*5 KO mice compared to WT, especially in hippocampus.

In details, in the hippocampus of KO mice (Figure 4E and Supplementary Table S1) a significant reduction of glutamine was observed compared to WT ($-22.6 \pm 4.6\%$; $p = 0.0044$), while glutamate was almost similar to WT mice ($-4.4 \pm 2.3\%$; $p = 0.281$). As a consequence, a defective glutamate to glutamine ratio was measured ($27.4 \pm 8.0\%$; $p = 0.017$).

In addition, creatine and phosphocreatine (Cr+PCr), whose levels reflect the adenosine triphosphate (ATP) metabolism at the intracellular level (Greenhaff, 2001), were significantly reduced ($-4.4 \pm 1.4\%$; $p = 0.028$) in *Cdkl5* KO animals. Similarly, the sum of NAA and its metabolite NAAG showed a decrease ($-11.2 \pm 2.5\%$, $p = 0.034$) in mutant mice that might reflect the presence of mitochondrial dysfunction or hypomyelination. On the same line, concentration of total choline (GPC+PCh), marker of myelination, neuronal function and mitochondrial oxidative metabolism, was notably reduced in KO mice compared to WT ($-14.9 \pm 2.5\%$ relative to WT; $p = 0.0015$). However, lactate was hardly detectable in KO as for WT mice, suggesting the absence of critical energy failure.

To assess the correlation between metabolic dysregulation and neuronal dysfunctions observed by MEMRI, MRS was also performed in the thalamus, where manganese contrast enhancement difference among groups was minor than in the hippocampus. In this cerebral region, MRS confirmed a decrease in some metabolites, although with a minor entity compared to the hippocampus (Figure 4J and Supplementary Table S1). In particular, as in the hippocampus, the total choline concentration (GPC+PCh) was significantly reduced ($-10.3 \pm 2.5\%$, $p = 0.034$) in KO mice. Moreover, a decreasing trend was observed in taurine levels ($-10.3 \pm 3.0\%$, $p = 0.077$) compared to WT.

Cdkl5 deficiency affects cellular energy metabolism in the hippocampus

In accordance with recent evidence (Pecorelli et al., 2015; Jagtap et al., 2019; Vigli et al., 2019), our MRS data highlighted a dysregulation of metabolites with a role in energy metabolism and oxidative stress, therefore suggesting a mitochondrial dysfunction in the *Cdkl5* null brain. To confirm this hypothesis, we used a luminescence assay to measure the ATP content in WT and KO hippocampi (Chida et al., 2012). As shown in Figure 5A, in the *Cdkl5* null hippocampus ATP levels are reduced of almost 35%, thus confirming previous results obtained in C57Bl/6J mice (Vigli et al., 2019). These data support our MRS findings of a metabolic dysfunction; we thus proceeded looking for the putative underlying molecular signatures.

Independently from fluctuations in the ATP demand, most eukaryotic cells maintain the nucleotide concentration at constant level. This is achieved through cellular systems able to monitor changes in ATP levels and to activate the molecular mechanisms necessary for restoring ATP homeostasis (Carling, 2017). Among these systems, AMP-activated protein kinase (AMPK) represents a key player that gets activated by Thr172 phosphorylation in response to a decrement in energy availability. We thus measured AMPK phosphorylation to investigate if the capacity of *Cdkl5* null hippocampus to respond to changes in cellular energy might be compromised. Indeed, we found a significant defect in AMPK Thr172 phosphorylation (Figure 5B).

Over 90% of the ATP produced in cells is generated by mitochondria; we thus proceeded analyzing whether mitochondrial mass could be compromised in the CD1 *Cdkl5* deficient mouse hippocampus, thus contributing to the reduced ATP content. To this purpose, by qPCR we measured the ratio between mitochondrial DNA (mtDNA) and nuclear DNA (nDNA). Our data (Figure 5C) indicated

that the mtDNA/nDNA ratio was not impaired in the hippocampus of KO mice with respect to WT. Unchanged mitochondrial density was found in *Cdkl5* adult mice maintained in a C57Bl/6J background (Supplementary Figure 2), thus supporting the result.

Excluding a different mitochondrial content between genotypes, we focused on electron transport chain and we used different molecular approaches to analyse in the CD1 KO hippocampus the expression of key genes involved in mitochondria functionality (Figure 6). In particular, we measured the expression of one gene for each subunit of the electron transfer chain (ETC) complexes. In KO animals, we observed a significant reduction in the mRNA levels of *Cox7b* (-31.1 ± 12.6%, p = 0.0159) (Figure 6A), codifying for Cytochrome C Oxidase Subunit 7B, belonging to Complex IV. Conversely, no change was observed in the transcriptional levels of genes codifying for subunits of the other complexes of the respiratory chain, such as *Ndufv2* (NADH dehydrogenase ubiquinone flavoprotein 2; Complex I), *Sdha* (succinate dehydrogenase; Complex II), *Uqrc1* (ubiquinol cytochrome c oxidoreductase chain 1, Complex III) and *Atp5a1* (ATP synthase F1 subunit alpha; Complex V).

Then, we analysed the expression of mitochondrial carriers belonging to the larger family of SLC25a transporters, which are in charge of transporting little molecules. Especially, considering their association with autism-related disorders (Anitha et al., 2012), we selected *Slc25a12* and *Slc25a27* genes, encoding for carrier Aralar and UCP4, respectively. We found a significant decrease in the transcriptional levels of *Slc25a27* in KO hippocampus (-18.7 ± 6.0%, p = 0.0269) (Figure 6B), and a decrement of *Slc25a12* expression that however did not reach statistical significance (-20.6 ± 7.2%, p = 0.0682) (Figure 6C).

In order to confirm these data at the protein level, by western blots we compared the expression levels of ETC complexes and SLC transporters between WT and *Cdkl5* null hippocampi (Figure 6D-F and Supplementary Figure S1). Interestingly, we confirmed a significant downregulation of Complex IV (Figure 6D), while the mitochondrial carriers did not exhibit significant defect (Figure 6E-F).

Discussion

CDKL5 deficiency is a neurodevelopmental disorder that is currently emerging as a frequent cause of epileptic seizures, severe intellectual disability and autistic symptoms in infants (Kothur et al., 2018;

Lindy et al., 2018). Mice that constitutively or conditionally lack *Cdkl5* recapitulate several features of the human disease, including autistic-like behaviours and hippocampal-dependent cognitive impairment (Wang et al., 2012; Amendola et al., 2014; Tang et al., 2017; Tang et al., 2019). However, the pathogenic mechanisms contributing to these phenotypes remain largely unknown and the field is still lacking quantitative, non-invasive and translational biomarkers that can be used to test drug efficacy. More recently, Mazziotti et al. have reported that visual evoked potentials (VEP) recorded from the visual cortex represent a useful biomarker for cortical circuit functions in *Cdkl5* defective mice (Mazziotti et al., 2017). Furthermore, recent clinical studies have proposed that cortical visual impairments or proxies of arousal fluctuations, such as pupillometry or heart rate variability, combined with deep learning, could be used as non-invasive and sensitive translational biomarkers for early detection of neurodevelopmental disorders, including CDD (Artoni et al., 2019; Demarest et al., 2019).

Neuroimaging is helpful to understand the pathophysiology of cognitive diseases. In particular, Magnetic Resonance Imaging (MRI) provides fine cerebral morphological information, while proton Magnetic Resonance Spectroscopy (MRS) determines the concentration of different metabolites in specific regions of the central nervous system. Since different metabolites are interlinked by their production and consumption, the overall neurochemical profile could be used as a fingerprint of a pathological condition. In addition, MRI and MRS are non-invasive tools that permit to monitor disease progression overtime and/or its stagnation or regression upon therapeutic intervention.

In this study, we have used different MR methods in order to analyze brain morphology and activity, to identify the cerebral regions predominantly affected by *Cdkl5* deficiency and to unveil metabolic alterations. We observed a dysregulation of several metabolites involved in energy and antioxidant metabolism in hippocampus; some of these alterations, such as reduced levels of total choline, were also confirmed in thalamus. Importantly, molecular studies confirmed MRS observations, corroborating the presence of mitochondrial impairment in the *Cdkl5* null hippocampus.

CDD can affect both genders and, although human data suggest that male patients might not be universally more severe (Demarest et al., 2019), in mice the heterozygous condition is generally associated with a milder phenotype with respect to that manifested by *Cdkl5* KO animals (Amendola

et al., 2014; Mazziotti et al., 2017). Thus, our study was mainly performed on adult (P70) *Cdkl5* null males.

Ex vivo and *in vivo* MRI analyses revealed that brain morphology is preserved in both genders, suggesting that mouse brain structure is not primarily affected by *Cdkl5* deficiency. Importantly, these results reconcile previous clinical reports debating whether *CDKL5* mutations cause atrophy (Akamine et al, 2018; Bodian et al., 2018; Liang et al., 2019; Mirzaa et al., 2013; Paine et al., 2012). So far, spontaneous seizures have only been detected in aged heterozygous *Cdkl5* mutant mice (Mulcaheya et al., 2020) and several CDD patients exhibit progressive cerebral atrophy that is often not present at the beginning of the pathology; therefore it is reasonable to assume that human brain changes are a secondary effect of the epileptic encephalopathy and/or its treatments, as already described for other genetic form, such as Dravet syndrome (Gaily et al., 2013).

In vivo MRS in the mouse brain is technically challenging and limited by the anesthesia duration, thus analysis can be performed in few predefined cerebral regions. To detect the most affected regions, we used MEMRI, which revealed a strong manganese accumulation through the entire *Cdkl5* deficient brain. Quantitative analysis indicated that in mutant brains manganese accumulates more consistently in hippocampus and visual system, therefore highlighting these brain regions as particularly susceptible to *Cdkl5* deficiency. Our results are in agreement with several behavioral studies that demonstrated learning and memory impairment together with anxiety and visual defects in *Cdkl5* deficient mice, as similarly observed in CDD patients (Amendola et al., 2014; Lupori et al., 2019; Okuda et al., 2018).

It is known that manganese enters into cells through voltage–gated calcium channels and activates glutamate receptors (e.g., N-methyl-D-aspartate receptors; NMDAR) (Itoh et al., 2008). Although additional molecular investigations are necessary to explain the mechanism of the increased manganese uptake in the *Cdkl5* null brain, enhanced NMDAR signaling and circuit hyper-excitability have already been described in the *Cdkl5* deficient hippocampus (Okuda et al., 2017; Tang et al., 2019). Furthermore, MEMRI can also reflect axonal sprouting and neuronal connectivity defects, as those reported in *Cdkl5* KO visual cortex (Pizzo et al., 2016). We thus suggest that MEMRI can be used as a measurable outcome in CDD preclinical studies to assess the effect of a treatment and to select brain regions, a possibility that we will investigate in the next future. The current MEMRI study

was done *ex vivo* in order to obtain maps of T1 relaxation time that allow quantitative analysis over the entire brain, but require long acquisition time to achieve high spatial resolution with an appropriate sensitivity. Nevertheless, MEMRI could be performed *in vivo* with the acquisition of T1 weighted images before and after manganese contrast infusion (Duong et al., 2000; Silva and Bock, 2008).

Since MEMRI revealed a stronger and more homogenous phenotype in *Cdkl5* KO males compared to females, we pursued with *in vivo* MRS only in KO animals, focusing on hippocampus. Visual system was excluded due to sensitivity limits of MRS in small regions and the difficulties to fit a voxel in the complex geometry. Instead, we analyzed metabolite concentration in thalamus, that, although less responsive to MEMRI, is an important center of sensory inputs whose relevance in CDD has been recently suggested (Lupori et al., 2019). Besides, it participates to the sleep-wake cycle regulation, often disturbed in CDD (Hagebeuk et al., 2012).

Interestingly, the multivariate analysis method of Partial Least Squares Discriminant Analysis (PLS-DA) reported a clear separation of the metabolic profile of *Cdkl5* KO mice from their respective controls, both in hippocampus and thalamus. The ability of MRS to discriminate *Cdkl5* null mice from WT encourages its use as a biomarker to investigate the capacity of a therapeutic treatment to restore, or at least redirect, the cerebral metabolism toward normal equilibrium. Of relevance, metabolic dysfunctions have already been reported in numerous neurological disorders, including autism (Stanley, 2002; Baruth et al., 2013; Siddiqui et al., 2016).

Specifically, our data reported a strong decrease in glutamine concentration and a reduction of both total creatine and NAA metabolites selectively in the hippocampus of KO mice. In addition, a consistent reduction of phosphocholine (PCh) with its catabolite glycerophosphocholine (GPC) was found both in the hippocampus and in the thalamus of *Cdkl5* mutant animals. Interestingly, these altered metabolites are closely related to mitochondrial functions and oxidative stress.

Indeed, glutamine has a pivotal role in mitochondrial ATP formation and its depletion induces defects in mitochondrial respiration (Piva and Mcevoy-Bowe 1998; Daurman, 2000; Fan et al., 2013). Glutamine is also a precursor of the antioxidant glutathione, one of the most important cellular antioxidants (Wang and Cynader, 2000) and it is required for synthesis of excitatory and inhibitory neurotransmitters, such as glutamate and GABA (Holcomb et al., 2000; Struzyńska and Sulkowski,

2004). PCh and GPC, besides their role in membrane synthesis and lipid metabolism, can affect mitochondrial activity (Schuler et al., 2016; Strifler et al., 2016) and abnormalities in choline metabolism have already been described in several diseases characterized by mitochondrial dysfunctions (Farber et al., 2000; Michel and Bakovic 2009). Moreover, since NAA is considered a neuronal putative marker and it is primarily synthesized within mitochondria, the observed reduction strengthens the evidence of mitochondrial impairment (Rossignol & Frye, 2011). *Cdkl5* null hippocampus showed also a notable decrease in total creatine concentration (Cr+PCr), which is essential in cell energy homeostasis (Wyss and Kaddurah-Daouk, 2000) and in cerebral osmoregulation (Bothwell et al., 2001). Of note, the normal lactate level in *Cdkl5* null brains suggests the lack of a severe energy failure, in line with the absence of epileptic seizures in this animal model.

We are aware that, in the next future, an extensive longitudinal study should be performed to better define the natural history of the observed metabolic dysregulation and to assess its value as measurable outcome. In particular, it would be of great interest to determine the onset of cerebral alterations and to establish whether the observed neurochemical profile could reflect disease severity and progression. Eventually, by including *Cdkl5* mutant females, we could contribute to understand whether the disease pattern overlaps in both genders, although with a possible delay in heterozygous females.

Our results are in line with recent evidence pointing out to a mitochondrial impairment in CDD. Indeed, an increase of 4HNE-Pas, a marker of lipid peroxidation-induced protein damage, and a reduction of NFE2L2, a regulator of cellular resistance to oxidants, were found in serum and fibroblasts of CDD patients (Pecorelli et al., 2015, 2011). Concomitantly, an aberrant mitochondrial function was described in isogenic neural progenitor cells (NPCs) derived from a CDD patient (Jagtap et al., 2019). Besides, analysis of mitochondrial functionality in *Cdkl5* null brain revealed defective mitochondrial respiratory activity and reduced ATP production, therefore confirming in the C57Bl/6J background our data and supporting the evidence of functional abnormalities in the cellular powerhouses (Vigli et al., 2019).

Mitochondria are critical organelles due to their role in producing energy, controlling Ca^{2+} signaling and generation of reactive oxygen species. Accordingly, mitochondrial dysfunction has devastating effects on the physiology of neurons and extensive studies have demonstrated mitochondrial defects

in many neuropsychiatric disorders, including autism (Castora, 2019; Reddy, 2009; Siddiqui et al., 2016). In line with this idea, we found it relevant to investigate whether defects in mitochondria number could concur to the observed metabolic defects. However, our molecular data indicated that the CD1 *Cdkl5* KO brain does not suffer from a variation in the organelle mass. EM quantifications performed in the null mice maintained in the C57Bl/6J strain showed that the hippocampus features physiological mitochondria density, thus providing a further evidence of similarities between the two strains modeling CDD (Supplementary Figure 2). Moreover, the same C57Bl/6J samples suggested that *Cdkl5* deficiency can affect mitochondrial size and cristae organization. Although it is not known if future studies in the CD1 background will reproduce the altered cristae phenotype observed in the C57Bl/6 strain, these EM findings provide additional evidence of mitochondrial defects associated with Cdkl5 deficiency. Although we willassess the progression of morphological and/or molecular mitochondrial phenotypes with cerebral development and ageing, these data prompted our molecular analyses. In fact, it is well known that respiratory chain complexes assemble into functional structures called supercomplexes (RCS), whose assembly and stability are affected by mitochondrial cristae shape (Cogliati et al., 2013). Interestingly, Vigli and colleagues have recently reported functional defects in complexes III-IV-V, therefore suggesting that ETC complexes may be indeed affected in the *Cdkl5* null mouse brains a result that well-fits with our data on mitochondrial ultrastructural defects (Vigli et al., 2019). Moreover, altered mitochondrial structures have been described in NPCs obtained from a 2-year-old female CDD patient carrying the truncating mutation 1412delT [pAsp471Ala; (Jagtap et al., 2019)], supporting the role of mitochondrial abnormalities in CDD. Finally, our data indicate a significant reduction of *Cox7b*, a Complex IV subunit that is indispensable for complex assembly and functioning as well as for mitochondrial oxidative phosphorylation, thus indicating for the first time a possible molecular substrate underlying mitochondrial dysfunctions. The observed transcriptional decrement of *Cox7b* appears in line with the already documented reduced expression of ETC genes in Rett syndrome (Gold et al., 2014), autism (Chauhan et al., 2011; Tang et al., 2013) and other neuropsychiatric disorders (Indrieri et al., 2012; Rezin et al., 2009), highlighting the importance of electron transport chain for CNS physiology.

It is well known that eukaryotic cells constantly adapt their metabolism in order to fulfill their energy needs. AMPK represents one of the most important factors able to sense low cellular ATP levels and

to respond increasing ATP generation and decreasing ATP consumption (Herzig & Shaw, 2018). Our data reveal that AMPK activation is defective in the *Cdkl5* null hippocampus, impairing the maintenance of ATP homeostasis. Of high relevance for CDD, AMPK is currently receiving a lot of attention as a potential target for treating diseases associated with metabolic dysfunctions, including neurological disorders (Curry et al., 2018).

In conclusion, our results have highlighted that MRI/MRS methods offer the opportunity to increase our comprehension of the cerebral dysfunctions that characterize mouse models of CDD and to identify biomarker(s) that can be exploited in preclinical settings to assess the efficacy of therapeutic approaches. Concerning the translational value of the identified measurable outcomes, at the very beginning of the disease (ranging from 2 to 12 months), most patients undergo brain MRI examinations that generally result unremarkable. However, we do not have any information about the long-term evolution of the human disorder. Therefore, even though limited by the necessity to perform exams in sedation, it would be of great interest to perform in CDD patients a prospective longitudinal study including brain MRI and MRS. Eventually, regarding the reported mitochondrial dysfunction, although preliminary data (Jagtap et al., 2019) have indicated that patients with CDD may show increased redox stress, it is evidently challenging to demonstrate mitochondrial impairment in human brain. However, we have identified deregulated genes/pathways that we believe contribute to the observed metabolic dysfunction and that might become useful to confirm overlapping phenotypes in human CDD tissues, neurons or organoids derived from patients' iPS cells. Eventually, the identified defect in AMPK activation strongly indicates the importance to promptly initiate a preclinical study testing the therapeutic potential of molecules targeting the AMPK signaling.

Conflict of interest

S.C., L.C., C.B., C.D.P., P.A., C.S., A.V., M.G., N.L. and A.F. have no competing interest to declare.

Funding

Author contribution

S.C. performed most of the experiments, analysed and interpreted the data, contributed to the writing of the manuscript and edited the manuscript. L.C. conducted MRI, MEMRI and MRS experiments, contributed to the writing of the manuscript and edited the manuscript. C.B. performed analysis of MEMRI acquisitions. C.D.P. supported in the selection of the methodological approaches for the analysis of mitochondrial defects and in interpretation of results. P.A. and C.S. conducted electron microscopy experiments. A.V. edited the manuscript. M.G. interpreted electron microscopy data and edited the manuscript. N.L directed the study, interpreted data, contributed to the conceptual design of the project, wrote the first draft of the manuscript and edited the manuscript. A.F. performed MEMRI experiment, interpreted the data, contributed to the conceptual design of the project, wrote the first draft of the manuscript and edited the manuscript.

Open Science Badges

This article has received a badge for *Open Materials* because it provided all relevant information to reproduce the study in the manuscript. More information about the Open Science badges can be found at https://cos.io/our-services/open-science-badges/

References

Akamine, S., Ishizaki, Y., Sakai, Y., Torisu, H., & Fukai, R. (2018). European Journal of Medical Genetics A male case with CDKL5 -associated encephalopathy manifesting transient methylmalonic acidemia. *European Journal of Molecular Genetics*, *61*(February), 451–454.

Amendola, E., Zhan, Y., Mattucci, C., Castroflorio, E., Calcagno, E., Fuchs, C., Lonetti, G., Silingardi, D., Vyssotski, A. L., Farley, D., Ciani, E., Pizzorusso, T., Giustetto, M., Gross, C. T. (2014). Mapping Pathological Phenotypes in a Mouse Model of CDKL5 Disorder. *PLoS ONE*, *9*(5), 5–16.

Anitha, A., Nakamura, K., Thanseem, I., Yamada, K., Iwayama, Y., Toyota, T., Matsuzaki, H., Miyachi, T., Yamada, S., Tsujii, M., Tsuchiya, K. T., Matsumoto, K., Iwata, Y., Suzuki, K., Ichikawa, H., Sugiyama, T., Yoshikawa, T., Mori, N. (2012). Brain region-specific altered expression and association of mitochondria-related genes in autism. *Molecular Autism*, *3*, 1–12.

Artoni, P., Piffer, A., Vinci, V., Leblanc, J., Nelson, C. A., & Hensch, T. K. (2019). Deep learning of spontaneous arousal fluctuations detects early cholinergic defects across neurodevelopmental mouse models and patients. *Proceedings of the National Academy of Sciences*, *131*, 2647–2661.

Artuso, R., Mencarelli, M. A., Polli, R., Sartori, S., Ariani, F., Pollazzon, M., Marozza, A., Cilio, M. R., Specchio, N., Vigevano, F., Vecchi, M., Boniver, C., Dalla Bernardina, B., Parmeggiani, A., Buoni, S., Hayek, G., Mari, F., Renieri, A., Murgia, A. (2010). Early-onset seizure variant of Rett syndrome: Definition of the clinical diagnostic criteria. *Brain and Development*, *32*(1), 17–24.

Bahi-Buisson, N., Nectoux, Ã. J., Haydee, Ã., Milh, Ã. M., Boddaert, N., Girard, B., Cances, C., Ville, D., Afenjar, A., Rio, M., Heron, D., N'GuyenMorel, M. A., Arzimanoglou, A., Philippe, C., Jonveaux, P., Chelly, J., Bienvenu, T. (2008). Key clinical features to identify girls with CDKL5 mutations. *Brain*, *131*, 2647–2661.

Balestra, D., Giorgio, D., Bizzotto, M., Fazzari, M., Zeev, B. Ben, Pinotti, M., Landsberger, N., Frasca, A. (2019). Splicing mutations impairing CDKL5 expression and activity can be efficiently rescued by U1snRNA-based therapy. *International Journal of Molecular Sciences*, *20*(17).

Barbiero, I., Peroni, D., Siniscalchi, P., Rusconi, L., Tramarin, M., De Rosa, R., Motta, P., Bianchi, M., Kilstrup-Nielsen, C. (2020). Pregnenolone and pregnenolone-methyl-ether rescue neuronal defects caused by dysfunctional CLIP170 in a neuronal model of CDKL5 Deficiency Disorder. *Neuropharmacology*, *164*(June 2019), 107897.

Baruth, J. M., Wall, C. A., Patterson, M. C., & Port, J. D. (2013). Proton Magnetic Resonance

Spectroscopy as a Probe into the Pathophysiology of Autism Spectrum Disorders (ASD): A Review. *Autism Research*, (February), 119–133.

Bodian, D. L., Schreiber, J. M., Vilboux, T., Khromykh, A., & Hauser, N. S. (2018). Mutation in an alternative transcript of CDKL5 in a boy with early-onset seizures. *Cold Spring Harbor Molecular Case Study*, 1–10.

Bothwell, J., Rae, C., Dixon, R., Styles, P., & Bhakoo, K. (2001). Hypo-osmotic Swelling-Activated Release of Organic Osmolytes in Brain Slices: Implications for Brain Oedema in Vivo. *Journal of Neurochemistry*, *77*(6), 1632–1640.

Carling, D. (2017). AMPK signalling in health and disease. *Current Opinion in Cell Biology*, *45*, 31-37.

Castora, F. J. (2019). Mitochondrial function and abnormalities implicated in the pathogenesis of ASD. *Progress in Neuropsychopharmacology & Biological Psychiatry*, *92*(September 2018), 83–108.

Chauhan, A., Gu, F., Essa, M. M., Wegiel, J., Kaur, K., Brown, W. T., & Chauhan, V. (2011). Brain region-specific deficit in mitochondrial electron transport chain complexes in children with autism. *Journal of Neurochemistry*, *117*(2), 209–220.

Chida, J., Yamane, K., Takei, T., & Kido, H. (2012). An efficient extraction method for quantitation of adenosine triphosphate in mammalian tissues and cells. *Analytica Chimica Acta*, *727*, 8–12.

Cobolli Gigli, C., Scaramuzza, L., Gandaglia, A., Bellini, E., Gabaglio, M., Parolaro, D., Kilstrup-Nielsen, C., Landsberger, N., Bedogni, F. (2016). MeCP2 related studies benefit from the use of CD1 as genetic background. *PLoS ONE*, *11*(4), 1–14.

Cogliati, S., Frezza, C., Soriano, M. E., Varanita, T., Quintana-Cabrera, R., Corrado, M., Cipolat, S., Costa, V., Casarin, A., Gomes, L. C., Perales-Clemente, E., Salviati, L., Fernandez-Silva, P., Enriquez, J. A., Scorrano, L. (2013). Mitochondrial cristae shape determines respiratory chain supercomplexes assembly and respiratory efficiency. *Cell*, *155*(1), 160–171.

Curry, D. W., Stutz, B., Andrews, Z. B., & Elsworth, J. D. (2018). Targeting AMPK Signaling as a Neuroprotective Strategy in Parkinson ' s Disease. *Journal of Parkinson's Disease*, *8*, 161–181.

Daurman, D. (2000). Role of glutamine depletion in severe illness. *Diabetes Nutr. Metab.*, *13*(1), 25–30.

Della Sala, G., Putignano, E., Chelini, G., Melani, R., Calcagno, E., Ratto, G. M., Amendola, E., Gross, C. T., Giustetto., M., Pizzorusso, T. (2016). Dendritic Spine Instability in a Mouse Model of CDKL5 Disorder Is Rescued by Insulin-like Growth Factor 1. *Biological Psychiatry*, *80*(4), 302–311.

Demarest, S. T., Olson, H. E., Moss, A., Knight, E. P., Zhang, X., Parikh, S., Swanson, L. C., Riley, K. D., Bazin, G. A., Angione, K., Niestroj, L. M., Lal, D., Juarez-Colunga, E., Benke, T. A. (2019). CDKL5 deficiency disorder : Relationship between genotype , epilepsy , cortical visual impairment , and development. *Epilepsia*, (December 2018), 1733–1742.

Duong, T. Q., Silva, A. C., Lee, S.-P., & Kim, S.-G. (2000). Functional MRI of Calcium-Dependent Synaptic Activity : Cross Correlation With CBF and BOLD Measurements. *Magnetic Resonance in Medicine*, *392*(43), 383–392.

Fan, J., Kamphorst, J. J., Mathew, R., Chung, M. K., White, E., Shlomi, T., & Rabinowitz, J. (2013). Glutamine-driven oxidative phosphorylation is a major ATP source in transformed mammalian cells in both normoxia and hypoxia. *Molecular Systems Biology*, *9*(712), 1–11.

Farber, S. A., Slack, B. E., & Blusztajn, J. A. N. K. (2000). Acceleration of phosphatidylcholine synthesis and breakdown by inhibitors of mitochondrial function in neuronal cells : a model of the membrane defect of Alzheimer ' s disease. *FASEB Journal*, *14*(14), 2198–2206.

Fehr, S., Wilson, M., Downs, J., Williams, S., Murgia, A., Sartori, S., Vecchi, M., Ho, G., Polli, R., Psoni, S., Bao, X., de Klerk, N., Leonard, H., Christodoulou, J. (2013). The CDKL5 disorder is an independent clinical entity associated with early-onset encephalopathy. *European Journal of Molecular Genetics*, *21*(3), 266–273.

Fuchs, C., Gennaccaro, L., Trazzi, S., Bastianini, S., Bettini, S., Lo Martire, V., Ren, E., Medici, G., Zoccoli, G., Rimondini, R., Ciani, E. (2018). Heterozygous CDKL5 Knockout Female Mice Are a Valuable Animal Model for CDKL5 Disorder. *Neural Plasticity*, *2018*.

Fuchs, C., Trazzi, S., Torricella, R., Viggiano, R., De Franceschi, M., Amendola, E., Gross, C., Calzà, L., Bartesaghi, R., Ciani, E. (2014). Neurobiology of Disease Loss of CDKL5 impairs survival and dendritic growth of newborn neurons by altering AKT / GSK-3 β signaling. *Neurobiology of Disease*, *70*, 53–68.

Gaily, E., Anttonen, A.-K., Valanne, L., Liukkonen, E., Traskelin, A.-L., Polvi, A., Lommi, M.,

Muona, M., Eriksson, K., Lehesjoki, A.-E. (2013). Dravet syndrome : New potential genetic modifiers , imaging abnormalities , and ictal findings. *Epilepsia*, *54*(9), 1577–1585.

Gandaglia, A., Brivio, E., Carli, S., Palmieri, M., Bedogni, F., Stefanelli, G., Bergo, A., Leva, B., Cattaneo, C., Pizzamiglio, L., Cicerone, M., Bianchi, V., Kilstrup-Nielsen, C., D'Annessa, I., Di Marino, D., D'Adamo, P., Antonucci, F., Frasca, A., Landsberger, N. (2018). A Novel Mecp2 Y120D Knock-in Model Displays Similar Behavioral Traits But Distinct Molecular Features Compared to the Mecp2 -Null Mouse Implying Precision Medicine for the Treatment of Rett Syndrome. *Molecular Neurobiology*, *56*(7), 4838-4854.

Gold, W. A., Williamson, S. L., Kaur, S., Hargreaves, I. P., Land, J. M., Pelka, G. J., Tam, P. P. L., Christodoulou, J. (2014). Mitochondrion Mitochondrial dysfunction in the skeletal muscle of a mouse model of Rett syndrome (RTT): Implications for the disease phenotype. *Mitochondrion*, *15*, 10–17.

Greenhaff, P. L. (2001). The creatine-phosphocreatine system: there's more than one song in its repertoire. *The Journal of Physiology, 537 (*Pt 3), 657.

Hagebeuk, E. E. O., van den Bossche, R. A., de Weerd, A. W. (2012). Respiratory and sleep disorders in female children with atypical Rett syndrome caused by mutations in the CDKL5 gene. *Developmental Medicine & Child Neurology*, *55*(5), 480–484.

Herzig, S., & Shaw, R. J. (2018). AMPK: guardian of metabolism and mitochondrial homeostasis. *Nature Reviews Molecular Cell Biology*, *19*(2), 121–135.

Holcomb, T., Taylor, L., Trohkimoinen, J., & Curthoys, N. P. (2000). Isolation, Characterization and Expression of a Human Brain Mitochondrial Glutaminase cDNA. *Molecular Brain Research*, *76*(1), 56–63.

Indrieri, A., Rahden, V. A. Van, Tiranti, V., Morleo, M., Iaconis, D., Tammaro, R., D'Amato, I., Conte, I., Maystadt, I., Demuth, S., Zvulunov, A., Kutsche, K., Zeviani, M., Franco, B. (2012). Mutations in COX7B Cause Microphthalmia with Linear Skin Lesions , an Unconventional Mitochondrial Disease. *The American Journal of Human Genetics*, *91*(5), 942–949.

Itoh, K., Sakata, M., Watanabe, M., Aikawa, Y., & Fujii, H. (2008). The entry of manganese ions into the brain is accelerated by the activation of N-methyl-d-aspartate receptors. *Neuroscience*, *154*(2), 732–740.

Jagtap, S., Thanos, J. M., Fu, T., Wang, J., Lalonde, J., Dial, T. O., Feiglin, A., Chen, J., Kohane, I., Lee, J. T., Sheridan, S. D., Perlis, R. H. (2019). Aberrant mitochondrial function in patient-derived neural cells from CDKL5 deficiency disorder and Rett syndrome. *Human Molecular Genetics*, *28*(21), 3625–3636.

Jhang, C., Huang, T., Hsueh, Y., & Liao, W. (2017). Mice lacking cyclin-dependent kinase-like 5 manifest autistic and ADHD-like behaviors. *Human Molecular Genetics*, *26*(20), 3922–3934.

King, A. J., Teki, S., & Willmore, B. D. B. (2018). Recent advances in understanding the auditory cortex. *F1000Research*, *7*(F-1000 Faculty Rev-1555).

Kothur, K., Holman, K., Farnsworth, E., Ho, G., Lorentzos, M., Troedson, C., Gupta, S., Webster, R., Procopis, P. G., Menezes, M. P., Antony, J., Arden-Holmes, S., Dale, R. C., Christodoulou, J., Gill, D., & Bennetts, B. (2018). Diagnostic yield of targeted massively parallel sequencing in children with epileptic encephalopathy. *Seizure: European Journal of Epilepsy*, *59*, 132–140.

Liang, J.-S., Huang, H., Wang, J., & Lu, J.-F. (2019). Phenotypic manifestations between male and female children with CDKL5 mutations. *Brain and Development*, *41*(9), 783–789.

Lindy, A. S., Stosser, M. B., Butler, E., Downtain-Pickersgill, C., Shanmugham, A., Retterer, K., Brandt, T., Gabriele, R. & Mcknight, D. A. (2018). Diagnostic outcomes for genetic testing of 70 genes in 8565 patients with epilepsy and neurodevelopmental disorders. *Epilepsia*, (March), 1062–1071.

Livak, K. J., & Schmittgen, T. D. (2001). Analysis of relative gene expression data using real-time quantitative PCR and the 2-ΔΔCT method. *Methods*, *25*(4), 402–408.

Lupori, L., Sagona, G., Fuchs, C., Stefanov, A., Putignano, E., Napoli, D., Strettoi, E., Ciani, E., & Pizzorusso, T. (2019). Site-specific abnormalities in the visual system of a mouse model of CDKL5 deficiency disorder. *Human Molecular Genetics*, *28*(17), 2851–61.

Mangatt, M., Wong, K., Anderson, B., Epstein, A., Hodgetts, S., Leonard, H., & Downs, J. (2016). Prevalence and onset of comorbidities in the CDKL5 disorder differ from Rett syndrome. *Orphanet Journal of Rare Diseases*, *11*(39).

Mazziotti, R., Lupori, L., Sagona, G., Gennaro, M., Della Sala, G., Putignano, E., & Pizzorusso, T. (2017). Searching for biomarkers of CDKL5 disorder : early-onset visual impairment in CDKL5 mutant mice. *Human Molecular Genetics*, *26*(12), 2290–2298.

Michel, V., & Bakovic, M. (2009). The solute carrier 44A1 is a mitochondrial protein and mediates choline transport. *The FASEB Journal*, *23*(8), 2749–2758.

Mirzaa, G. M., Paciorkowski, A., Marsh, E. D., Berry-Kravis, E. M., Medne, L., Grix, A., Wirrel., E. C., Powell, B., R., Nickels, K., C., Burton, B., Paras, A., Kim, K., Chung, W., Dobyns, W. B., & Das, S. (2013). CDKL5 and ARX mutations in males with early-onset epilepsy. *Pediatric Neurology*, *48*(5), 367–377.

Moseley, B. D., Dhamija, R., Wirrell, E. C., & Nickels, K. C. (2012). Pediatric Neurology Historic , Clinical , and Prognostic Features of Epileptic Encephalopathies Caused by CDKL5 Mutations. *Pediatric Neurology*, *46*(2), 101–105.

Mulcaheya, P., Tang, S., Takano, H., White, A., Davila Portillo, D., Kane, O. M., Marsh, E. D., Zhou, Z., & Coulter, D. A. (2020). Aged heterozygous Cdkl5 mutant mice exhibit spontaneous epileptic spasms. *Experimental Neurology*, *332*, 113388.

Okuda, K., Kobayashi, S., Fukaya, M., Watanabe, A., Murakami, T., Hagiwara, M., Sato, T., Ueno, H., Ogonuki, N., Komano-Inoue, S., Manabe, H., Yamaguchi, M., Ogura, A., Asahara, H., Sakagami, H., Mizuguchi, M., Manabe, T., & Tanaka, T. (2017). CDKL5 controls postsynaptic localization of GluN2B-containing NMDA receptors in the hippocampus and regulates seizure susceptibility. *Neurobiology of Disease*, *106*, 158–170.

Okuda, K., Takao, K., Watanabe, A., Miyakawa, T., Mizuguchi, M., & Tanaka, T. (2018). Comprehensive behavioral analysis of the Cdkl5 knockout mice revealed significant enhancement in anxiety- and fear-related behaviors and impairment in both acquisition and long-term retention of spatial reference memory. *PLoS ONE*, *13*(4), 1–34.

Paine, S., Munot, P., Carmichael, J., Das, K., Weber, M. A., Prabhakar, P., & Jacques, T. (2012). The neuropathological consequences of CDKL5 mutation. *Neuropathology and Applied Neurobiology*, *38*, 744–747.

Pecorelli, A., Belmonte, G., Meloni, I., Cervellati, F., Sticozzi, C., De Felice, C., Signorini, C., Cortellazzo, A., Leoncini, S., Ciccoli, L., Renieri, A., Forman, H. J., Hayek, J., & Valacchi, G. (2015). Alteration of serum lipid profile, SRB1 loss, and impaired Nrf2 activation in CDKL5 disorder. *Free Radic Biol Med*, *86*, 156–165.

Pecorelli, A., Ciccoli, L., Signorini, C., Leoncini, S., Giardini, A., D'Esposito, M., Filosa, S., Hayek,

J., De Felice, C., & Valacchi, G. (2011). Increased levels of 4HNE-protein plasma adducts in Rett syndrome. *Clinical Biochemistry*, *44*(5–6), 368–371.

Pho, G. N., Goard, M. J., Woodson, J., Crawford, B., & Sur, M. (2019). Task-dependent representations of stimulus and choice. *Nature Communications*, *10*(1), 389.

Piva, T., & Mcevoy-Bowe, E. (1998). Oxidation of glutamine in HeLa cells: role and control of truncated TCA cycles in tumour mitochondria. *Journal of Cell Biochemistry*, *68*, 213–225.

Pizzo, R., Gurgone, A., Castroflorio, E., Amendola, E., Gross, C., Sassoè-pognetto, M., & Giustetto, M. (2016). Lack of Cdkl5 Disrupts the Organization of Excitatory and Inhibitory Synapses and Parvalbumin Interneurons in the Primary Visual Cortex. *Frontiers in Cellular Neuroscience*, *10*(November), 1–16.

Reddy, P. H. (2009). The role of mitochondria in neurodegenerative diseases: mitochondria as a therapeutic target in Alzheimer's disease P. *CNS Sectr.*, *14*(8 Supll 7), 8–18.

Ren, E., Roncacé, V., Trazzi, S., Fuchs, C., Medici, G., Gennaccaro, L., Loi, M., Galvani, G., Ye, K., Rimondini, R., Aicardi, G., & Ciani, E. (2019). Functional and Structural Impairments in the Perirhinal Cortex of a Mouse Model of CDKL5 Deficiency Disorder Are Rescued by a TrkB Agonist. *Frontiers in Cellular Neuroscience*, *13*(April), 169.

Rezin, G., Amboni, G., Zugno, A., Quevedo, J., & Streck, E. (2009). Mitochondrial dysfunction and psychiatric disorders. *Neurochemical Research*, *34*, 1021–1029.

Rossignol, D. A., & Frye, R. E. (2011). Mitochondrial dysfunction in autism spectrum disorders : a systematic review and meta-analysis. *Molecular Psychiatry*, *17*(3), 290–314.

Rusconi, L., Salvatoni, L., Giudici, L., Bertani, I., Kilstrup-nielsen, C., Broccoli, V., & Landsberger, N. (2008). CDKL5 Expression Is Modulated during Neuronal Development and Its Subcellular Distribution Is Tightly Regulated by the C-terminal Tail . *The Journal of Biological Chemistry*, *283*(44), 30101–30111.

Schroeder, E., Yuan, L., Seong, E., Ligon, C., Dekorver, N., Gurumurthy, C. B., & Arikkath, J. (2019). Neuron-Type Specific Loss of CDKL5 Leads to Alterations in mTOR Signaling and Synaptic Markers. *Molecular Neurobiology*, *56*, 4151–4162.

Schuler, M., Di Bartolomeo, F., Mårtensson, C. U., Daum, G., & Becker, T. (2016). Phosphatidylcholine Affects Inner Membrane Protein Translocases of Mitochondria. *The Journal*

of Biological Chemistry, *291*(36), 18718–18729.

Siddiqui, M. F., Elwell, C., & Johnson, M. H. (2016). Mitochondrial Dysfunction in Autism Spectrum Disorders. *Autism Open Access*, *6*(5).

Siegmund, S. E., Grassucci, R., Carter, S. D., Barca, E., Farino, Z. J., Juanola-Falgarona, M., Zhang, P., Tanji, K., Hirano, M., Schon, E. A., Frank, J., & Freyberg, Z. (2018). Three-Dimensional Analysis of Mitochondrial Crista Ultrastructure in a Patient with Leigh Syndrome by In Situ Cryoelectron Tomography. *IScience*, *6*, 83–91.

Silva, A. C., & Bock, N. A. (2008). Manganese-Enhanced MRI : An Exceptional Tool in Translational Neuroimaging. *Schizophrenia Bulletin*, *34*(4), 595–604.

Stanley, A. (2002). In Vivo Magnetic Resonance Spectroscopy and Its Application to Neuropsychiatric Disorders. *Journal of Psychiatry*, *47*(4).

Strifler, G., Tuboly, E., Gorbe, A., Boros, M., Pecz, D., & Hartmann, P. (2016). Targeting Mitochondrial Dysfunction with L- Alpha Glycerylphosphorylcholine. *PLoS ONE*, 1–14.

Struzyńska, L., & Sulkowski, G. (2004). Relationships Between Glutamine, Glutamate, and GABA in Nerve Endings Under Pb-toxicity Conditions. *Journal Inorganic Biochemistry*, *98*(6), 951–958.

Tang, G., Rios, P., Kuo, S.-H., Akman, H., Rosoklija, G., Tanji, K., Dwork, A., Schon, E. A., Dimauro, S., Goldman, J., & Sulzer, D. (2013). Mitochondrial abnormalities in temporal lobe of autistic brain. *Neurobiology*, *54*, 349–361.

Tang, S., Terzic, B., Wang, I. J., Sarmiento, N., Sizov, K., Cui, Y., Takano, H., Marsh, E. D., Zhou, Z., & Coulter, D. A. (2019). Altered NMDAR signaling underlies autistic-like features in mouse models of CDKL5 deficiency disorder. *Nature Communications*, *10*(1), 2655.

Tang, X. S., Wang, I. J., Yue, C., Takano, H., Terzic, B., Pance, X., Lee, J. Y., Coulter, D. A., & Zhou, Z. (2017). Loss of CDKL5 in Glutamatergic Neurons Disrupts Hippocampal Microcircuitry and Leads to Memory Impairment in Mice. *Neurobiology of Disease*, *37*(31), 7420–7437.

Trovò, L., Fuchs, C., De Rosa, R., Barbiero, I., Tramarin, M., Ciani, E., Rusconi, L., & Kilstrup-Nielsen, C. (2020). The green tea polyphenol epigallocatechin-3-gallate (EGCG) restores CDKL5-dependent synaptic defects in vitro and in vivo. *Neurobiology of Disease*, *138*(August 2019), 104791.

Vigli, D., Rusconi, L., Valenti, D., La Montanara, P., Cosentino, L., Lacivita, E., Leopoldo, M., Amendola, E., Gross, C., Landsberger, N., Laviola, G., Kilstrup-Nielsen, C., Vacca, R. A., & De Filippis, B. (2019). Rescue of prepulse inhibition de fi cit and brain mitochondrial dysfunction by pharmacological stimulation of the central serotonin receptor 7 in a mouse model of CDKL5 Deficiency Disorder. *Neuropharmacology*, *144*(July 2018), 104–114.

Wang, I. J., Allen, M., Goffin, D., Zhu, X., Fairless, A. H., Brodkin, E. S., Siegel, S. J., Marsh, E. D., Blendy, J. A., & Zhou, Z. (2012). Loss of CDKL5 disrupts kinome pro fi le and event-related potentials leading to autistic-like phenotypes in mice. *Proceedings of the American Thoracic Society*, *109*(52), 21516–21521.

Wang, X. F., & Cynader, M. S. (2000). Astrocytes Provide Cysteine to Neurons by Releasing Glutathione. *Journal of Neurochemistry*, *74*, 1434–1442.

White, R., Ho, G., Schmidt, S., Scheffer, I. E., Fischer, A., Yendle, S. C., Bienvenu, T., Nectoux, J., Ellaway, C. J., Darmanian, A., Tong, X., Cloosterman, D., Bennetts, B., Kalra, V., Fullston, T., Gecz, J., Cox, T. C., & Christodoulou, J. (2010). Cyclin-dependent kinase-like 5 (CDKL5) mutation screening in Rett syndrome and related disorders. *Twin Research and Human Genetics*, *13*(2), 168–178.

Wyss, M., & Kaddurah-Daouk, R. (2000). Creatine and Creatinine Metabolism. *Physiological Reviews*, *80*(3), 1107–1213.

Xia, J., & Wishart, D. S. (2011). Web-based inference of biological patterns, functions and pathways from metabolomic data using MetaboAnalyst. *Nature Protocols*.

Zhu, Y. C. , & Xiong, Z. Q. (2018). Molecular and Synaptic Bases of CDKL5 Disorder. *Developmental Neurolobiology*, *79*(1), 8–19.

Figure Legends

Figure 1. Time flow of the animals used in the study.

Figure 2. *Cdkl5* **KO and HET mice do not manifest cerebral atrophy.** (A, B) *Ex vivo* MRI on CD1 male (blue, n: WT = 6, KO = 5, P70) and female (violet, n: WT = 8, HET = 10, P160-195) mutants displayed identical cerebral area along the different sections and total volume. Olfactory bulbs and cerebellum were excluded from the analyses as they were partially damaged during brain extraction procedures. (C) The weight of extracted brains was also similar among all groups. (D) *In vivo* MRI did not reveal any anatomical abnormality and confirmed a perfect matching between CD1 KO and WT brains. (E) Representative T2 weighted MR images of slices 10 to 13 from WT and KO brains obtained *in vivo.* All graphs represent mean ± SEM.

Figure 3. MEMRI highlights hyperactive areas in *Cdkl5* **mutant brains.** (A) Graphical representation of MEMRI: after systemic administration of $MnCl_2$, Mn^{2+} ions enter excitable cells primarily through voltage-gated calcium channels $Ca_v1.2$ and accumulate inside neurons. As a contrast agent, Mn^{2+} can be detected by MRI, revealing the neuronal activity of specific cerebral regions. (B) Representative T2 weighted MR images of a mouse used as anatomical reference to define brain areas (first column) and maps of relaxivity (1/T1, colored images) from blank, WT, *Cdkl5* KO and HET mice used to quantify manganese uptake. EP: entorhinal-perirhinal cortex; H: hippocampus; Opt: optic tract; PF: parafascicular nucleus of the thalamus; SC: superior colliculus; SS: somatosensory cortex; VC: visual cortex; VP: ventral posterior nucleus of the thalamus.

Figure 4. *In vivo* **MRS reveals a metabolic dysregulation in** *Cdkl5* **KO mice.** Voxel placement from hippocampus (A) and thalamus (F) of a KO and WT mouse. (B, G) Score plots from the Partial Least-Squares Discriminant Analysis (PLS-DA) indicate the metabolic profile differences between WT and *Cdkl5* KO animals. (C, H) Metabolites having the most relevant influence to groups discrimination are identified by a VIP score >1.2. (D, I) Representative MRS spectra from KO (light blue) and WT (dark blue) mouse and the concentration of key metabolites is reported. In particular, in hippocampus (E), Cr+PCr, glutamine, GPC+PCh, Glu/Gln ratio, and NAA+NAAG are significantly deregulated. In thalamus (J), GPC+PCh levels are significantly reduced, while taurine shows a decreasing trend.

Cr: Creatine; Glu: glutamate; Gln: Glutamine; GPC: glycerophosphocholine; PCh: phosphocholine; PCr: phosphocreatine; NAA: N-acetyl-aspartate; NAAG: N-acetyl-aspartyl-glutamate. Statistical significance assessed by Mann-Whitney U-test (Glu in the hippocampus and Cr+PCr in the thalamus) or Student's t test (Cr+PCr, Gln, GPC+PCh, Glu/Gln, NAA+NAAG and Tau in the hippocampus; Glu, Gln, GPC+PCH, Glu/Gln, NAA+NAAG and Tau in the thalamus), in accordance with D'Agostino-Pearson normality test for data distribution: * $p < 0.05$, ** $p < 0.01$ and \$ $p = 0.077$. All graphs represent mean ± SEM (n = 7 WT and 8 KO).

Figure 5. The *Cdkl5* deficient hippocampus manifests evident defects in ATP homeostasis (A) CellTiter Glo assay revealed a significant reduction of ATP levels in *Cdkl5* KO (n = 5) hippocampus compared to WT littermates (n = 5). (B) Bar graph shows that the ratio of pAMPK/AMPK is significantly decreased in the hippocampus of *Cdkl5* KO (n = 9) with respect to WT (n = 9). Values are reported as arbitrary units. Right panel shows a representative Western Blots of total AMPK and phosphorylated AMPK (pAMPK Thr172). (C) The mtDNA/nDNA was calculated in the hippocampus of WT (n = 6) and *Cdkl5* KO (n = 5) animals. Data are reported as mean ± SEM and expressed as percentage of WT. Statistical significance assessed by Student's t test: * $p < 0.05$, ** $p < 0.01$, *** $p < 0.001$ and **** $p < 0.0001$. All graphs represent mean ± SEM.
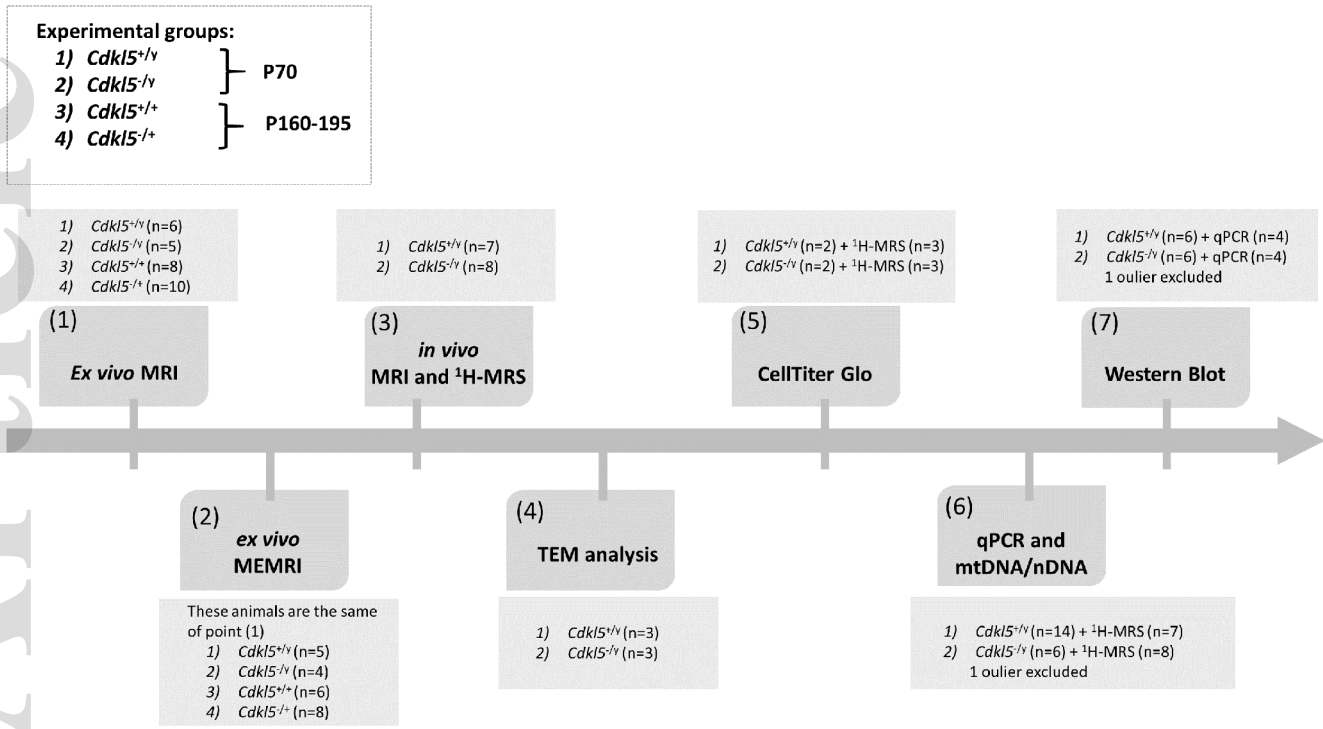
Figure 6. *Cdkl5* KO brains display an aberrant expression of complex IV of the electron transport chain. (A-C) The transcriptional expression of mitochondrial genes was analyzed by quantitative RT-PCR in WT and KO hippocampi (n = 15 WT and 8 KO). Results displayed a consistent reduction of *Cox7b* and *Slc25a27*, while *Slc25a12* showed a decreasing trend. *Hprt* was used as internal standard. The fold changes of transcript levels, compared to WT animals, are reported as mean ± SEM (\$ $p < 0.068$; * $p < 0.05$; by Mann-Whitney U test or Student's t test, in accordance with distribution of data). (D-F) Western blots of mitochondrial proteins from WT and KO mice. A significant decrease was confirmed for the complex IV of the ETC, Cox7b. Bar graphs show the mean ± SEM of the expression levels in *Cdkl5* KO compared to WT, of ETCs (total OXPHOS) (n = 10 WT, n = 9 KO), Slc25a27 (UCP4) (n = 9 WT, n = 9 KO) and Slc25a12 (Aralar) (n= 6 WT, n= 6 KO). Full blots are reported in Supplementary Figure S1. Statistical significance was assessed by Student's t test

(*Ndufv2, Sdha, Uqrc1, Atp5a1*, *Slc25a27* and *Slc25a12* in quantitative RT-PCR and ETC complexes and Slc25a12 in Western Blot*)* or Mann-Whitney U test (*Cox7b* in quantitative RT-PCR and Slc25a27 in Western Blot), in accordance with D'Agostino-Pearson test for data distribution; * p <0.05.
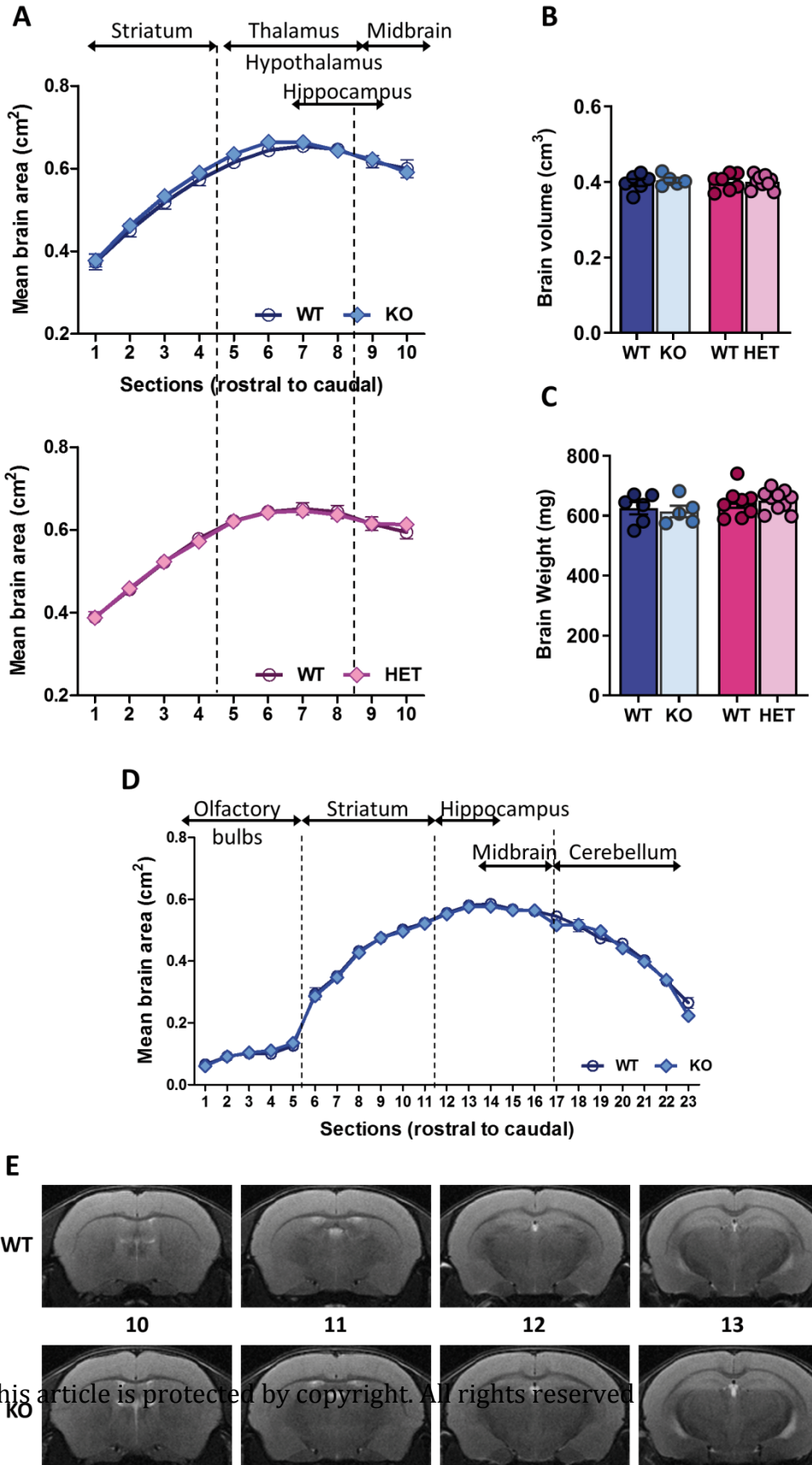
Table 1. Manganese contrast enhancement in *Cdkl5* mutant brain. The values indicate the difference of manganese uptake in *Cdkl5* KO (n= 4) and HET brains (n=8) compared to their WT littermates (n= 5 males and n=6 females) 24 h after $MnCl_2$ administration (60 mg/kg, i.p.).
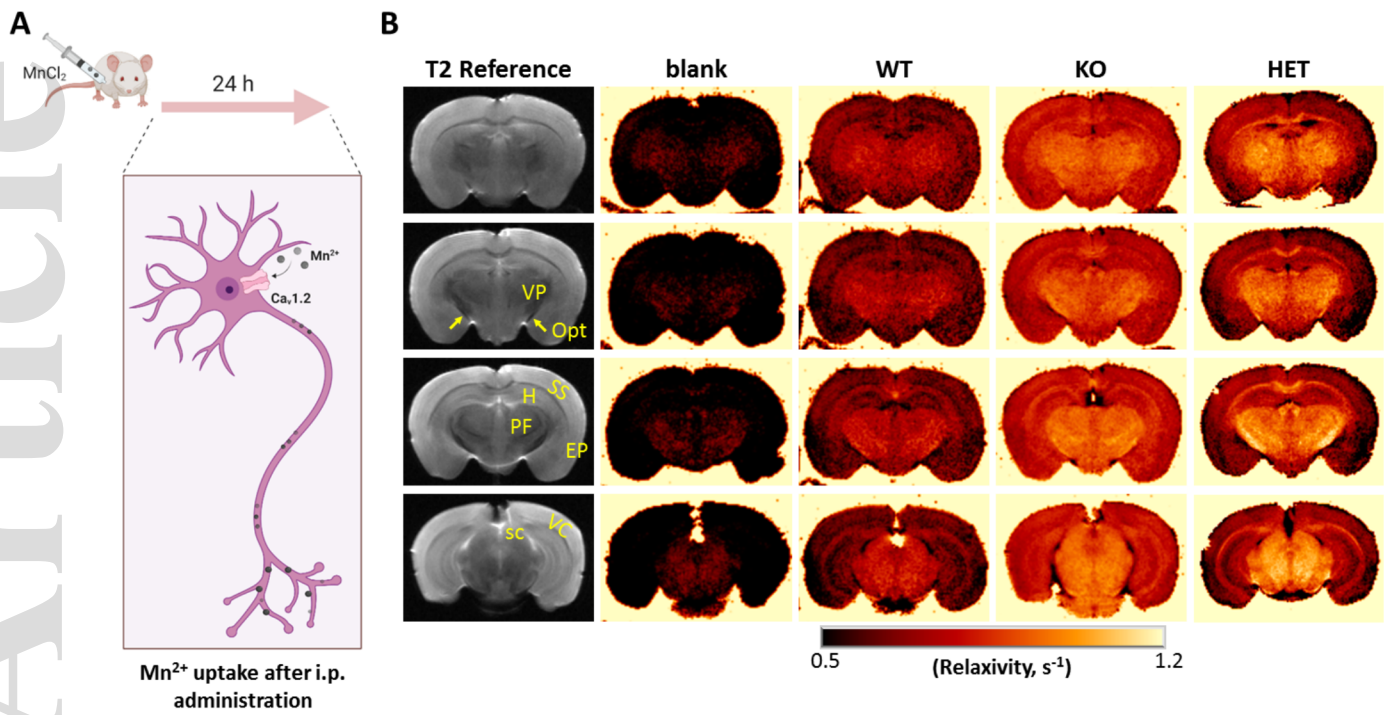
% Enhancement compared to WT (mean± SEM)		Male		Female	
		KO	p value	HET	p value
	Hippocampus	47.3 ± 14.6	**0.0286***	21.7 ± 5.1	0.268
Cerebral Cortex	Auditory cortex	21.5 ± 8.6	**0.0286***	43.0 ± 5.6	**0.0177***
	Entorhinal-Perirhinal (EP) cortex	36.3 ± 17.4	0.114	77.3 ± 6.1	**0.0025****
	Piriform cortex	47.7 ± 19.3	0.114	17.2 ± 6.3	0.432
	Posterior parietal association area	34.2 ± 13.2	0.057$	22.5 ± 6.1	0.202
	Retrosplenial cortex	35.2 ± 16.2	0.200	18.5 ± 7.7	0.432
	Somatosensorial cortex (SS)	31.3 ± 14.1	0.0826	22.4 ± 6.1	0.1042
Thalamus	Parafascicular nucleus (PF)	35.1 ± 10.5	0.114	14.1 ± 5.3	0.149
	Ventral posterior nucleus (VP)	34.5 ± 15.2	0.114	26.8 ±5.9	0.106
Visual System	Optic tract (Opt)	16.8 ±13.5	0.486	-9.7 ± 4.0	0.149
	Superior Colliculus (SC)	71.8 ± 25.6	**0.0286***	27.7 ± 6.1	**0.0303***
	Visual cortex (VC)	58.1 ± 31.5	0.114	63.4 ± 7.1	**0.0025****
	Hypothalamus	54.8 ± 8.9	0.057$	-6.9 ± 7.6	0.432

Mann-Whitney U test: * p < 0.05, ** p <0.01, $ p = 0.057.

Experimental groups:
1) *Cdkl5*$^{+/y}$
2) *Cdkl5*$^{-/y}$ — P70
3) *Cdkl5*$^{+/+}$
4) *Cdkl5*$^{-/+}$ — P160-195

1) *Cdkl5*$^{+/y}$ (n=6)
2) *Cdkl5*$^{-/y}$ (n=5)
3) *Cdkl5*$^{+/+}$ (n=8)
4) *Cdkl5*$^{-/+}$ (n=10)

(1) *Ex vivo* MRI

1) *Cdkl5*$^{+/y}$ (n=7)
2) *Cdkl5*$^{-/y}$ (n=8)

(3) *in vivo* MRI and ^{1}H-MRS

1) *Cdkl5*$^{+/y}$ (n=2) + ^{1}H-MRS (n=3)
2) *Cdkl5*$^{-/y}$ (n=2) + ^{1}H-MRS (n=3)

(5) CellTiter Glo

1) *Cdkl5*$^{+/y}$ (n=6) + qPCR (n=4)
2) *Cdkl5*$^{-/y}$ (n=6) + qPCR (n=4)
1 oulier excluded

(7) Western Blot

(2) *ex vivo* MEMRI

These animals are the same of point (1)
1) *Cdkl5*$^{+/y}$ (n=5)
2) *Cdkl5*$^{-/y}$ (n=4)
3) *Cdkl5*$^{+/+}$ (n=6)
4) *Cdkl5*$^{-/+}$ (n=8)

(4) TEM analysis

1) *Cdkl5*$^{+/y}$ (n=3)
2) *Cdkl5*$^{-/y}$ (n=3)

(6) qPCR and mtDNA/nDNA

1) *Cdkl5*$^{+/y}$ (n=14) + ^{1}H-MRS (n=7)
2) *Cdkl5*$^{-/y}$ (n=6) + ^{1}H-MRS (n=8)
1 oulier excluded

jnc_15300_f1.tif

A

Striatum   Thalamus   Midbrain
            Hypothalamus
                Hippocampus

WT   KO

D

Olfactory   Striatum   Hippocampus
bulbs
                    Midbrain   Cerebellum

WT   KO

B

C

E

WT

10   11   12   13

KO

A

MnCl₂

24 h

Mn²⁺
Caᵥ1.2

Mn²⁺ uptake after i.p.
administration

B

| T2 Reference | blank | WT | KO | HET |

VP   Opt

H SS
PF
EP

sc VC

0.5   (Relaxivity, s⁻¹)   1.2

jnc_15300_f3.tif

jnc_15300_f4.tif

A ATP levels

B pAMPK/AMPK

C mtDNA/nDNA

jnc_15300_f5.tif

jnc_15300_f6.tif